

Article

New Syntheses, Analytic Spin Hamiltonians, Structural and Computational Characterization for a Series of Tri-, Hexa- and Hepta-Nuclear Copper (II) Complexes with Prototypic Patterns

Ana Maria Toader ¹, Maria Cristina Buta ¹, Fanica Cimpoesu ^{1,*}, Andrei-Iulian Toma ², Christina Marie Zalaru ³, Ludmila Otilia Cinteza ⁴ and Marilena Ferbinteanu ^{2,*}

¹ Institute of Physical Chemistry, Splaiul Independentei 202, 060021 Bucharest, Romania; ancutatoader@yahoo.fr (A.M.T.); butamariacristina@gmail.com (M.C.B.)

² Department of Inorganic Chemistry, Faculty of Chemistry, University of Bucharest, Dumbrava Rosie 23, 020462 Bucharest, Romania; andreitoma119@yahoo.com

³ Department of Organic Chemistry, Biochemistry and Catalysis, Faculty of Chemistry, University of Bucharest, Panduri 90-92, 050663 Bucharest, Romania; christina.zalaru@chimie.unibuc.ro

⁴ Physical Chemistry Department, University of Bucharest, 030118 Bucharest, Romania; ocinteza@gw-chimie.math.unibuc.ro

* Correspondence: cfanica@yahoo.com (F.C.); marilena.cimpoesu@g.unibuc.ro (M.F.); Tel.: +40-21-312-1147 (F.C.); +40-21-210-3495 (M.F.)

Abstract: We present a series of pyrazolato-bridged copper complexes with interesting structures that can be considered prototypic patterns for tri-, hexa- and hepta- nuclear systems. The trinuclear shows an almost regular triangle with a μ_3 -OH central group. The hexanuclear has identical monomer units, the Cu_6 system forming a regular hexagon. The heptanuclear can be described as two trinuclear moieties sandwiching a central copper ion via carboxylate bridges. In the heptanuclear system, the pyrazolate bridges are consolidating the triangular faces, which are sketching an elongated trigonal antiprism. The magnetic properties of these systems, dominated by the strong antiferromagnetism along the pyrazolate bridges, were described transparently, outlining the energy levels formulas in terms of Heisenberg exchange parameters J , within the specific topologies. We succeeded in finding a simple Kambe-type resolution of the Heisenberg spin Hamiltonian for the rather complex case of the heptanuclear. In a similar manner, the weak intermolecular coupling of two trimer units (aside from the strong exchange inside triangles) was resolved by closed energy formulas. The hexanuclear can be legitimately proposed as a case of coordination-based aromaticity, since the phenomenology of the six-spins problem resembles the bonding in benzene. The Broken-Symmetry Density Functional Theory (BS-DFT) calculations are non-trivial results, being intrinsically difficult at high nuclearities.

Keywords: trinuclear complex; hexamer metallacycle; heptanuclear complex; pyrazolato-bridged ligand systems; spin Hamiltonian; spin models; Kambe-type energy formulas; Broken-Symmetry Density Functional Theory calculations



Citation: Toader, A.M.; Buta, M.C.; Cimpoesu, F.; Toma, A.-I.; Zalaru, C.M.; Cinteza, L.O.; Ferbinteanu, M. New Syntheses, Analytic Spin Hamiltonians, Structural and Computational Characterization for a Series of Tri-, Hexa- and Hepta-Nuclear Copper (II) Complexes with Prototypic Patterns. *Chemistry* **2021**, *3*, 411–439. <https://doi.org/10.3390/chemistry3010031>

Received: 28 January 2021

Accepted: 4 March 2021

Published: 15 March 2021

Publisher's Note: MDPI stays neutral with regard to jurisdictional claims in published maps and institutional affiliations.



Copyright: © 2021 by the authors. Licensee MDPI, Basel, Switzerland. This article is an open access article distributed under the terms and conditions of the Creative Commons Attribution (CC BY) license (<https://creativecommons.org/licenses/by/4.0/>).

1. Introduction

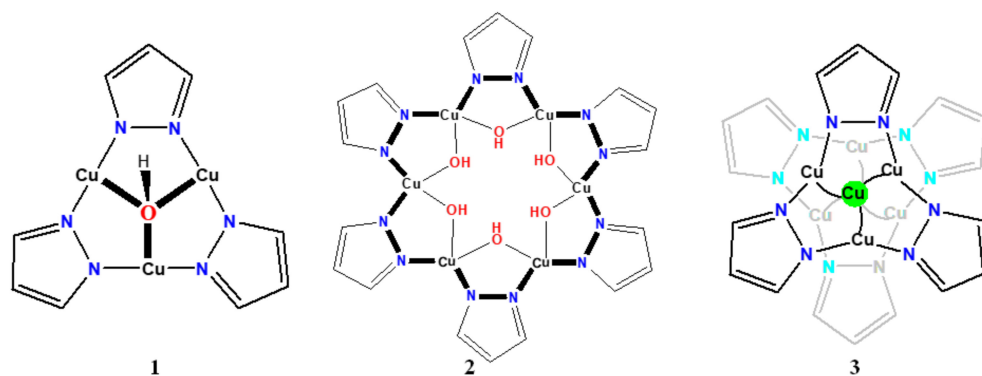
This work is built on the frame of our deals in structural chemistry [1], putting on equal footing the interest for experimental data from new syntheses (followed by X-ray characterization) and theoretical approaches (phenomenological or computational). We will present a suite of copper complexes having prototypical structural patterns, rising and solving important aspects of their molecular magnetism. The common feature of all the presented systems is the presence of pyrazolato-bridges in their polynuclear edifices.

The coordination chemistry of the pyrazole-based ligands provides a variety of compounds with a large spectrum of molecular geometries, nuclearities and interesting properties [2]. Pyrazole and its derivatives proved to be versatile ligands, exhibiting several

coordination modes [3], the bridging functionality allowing to form polynuclear structures [4]. Polynuclear copper complexes attracted special attention due to their magnetic properties and for their relevance to the biomimetics of the copper proteins (e.g., ascorbate oxidase, laccase, ceruloplasmin, methane monooxygenase) [5]. Among them, the triangular trinuclear copper complexes were highlighted for their physical and chemical properties related with blue multicopper oxidases [6–8].

From the magnetic point of view, the cyclic trinuclear copper systems were regarded as geometrically frustrated antiferromagnetic compounds, offering the possibility to test the exchange coupling models [9,10]. In the last decades, density functional theory (DFT) methods and especially the broken-symmetry approach were raised as instruments of choice to evaluate the magnetic coupling parameters for such systems [11]. There are several electronic structure calculations on a cyclic trinuclear copper system, done on model systems [12,13] or on experimental molecules [14,15]. In this work we will corroborate the magnetic measurements with computational quests, performing and discussing non-trivial numeric experiments.

The patterns of the discussed compounds are shown in Scheme 1, the labeling of frames corresponding to those of the presented structures. While there are several known trinuclear [16–18] and hexa-nuclear [19–23] analogs of the reported compounds, the heptanuclear congeners are rare [24,25]. The insight offered by the phenomenological and computational analyses is rather unprecedented, fixing landmarks on account of the discussed systems, considering that each compound is a representative of their given structural pattern.



Scheme 1. Structural patterns of compounds 1, 2 and 3.

The triangular copper complexes with a hydroxy- or oxo-trinuclear bridge were obtained usually by the pyrazole deprotonation in the presence of a base [16–18], while in the case of using carboxylates copper salts, the pyrazole deprotonation is favored by the presence of carboxylate ions. Our compound 1 parallels literature results in terms of synthetic procedures and outcomes [26,27].

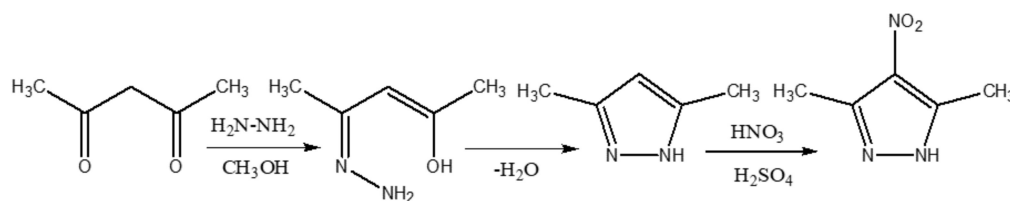
Concretely, we used the reaction of copper (II) acetate with 3,5-dimethyl-4-nitropyrazole (dmnpz) in protic solvents to obtain a new triangular trinuclear copper complex, $[\text{Cu}_3(\mu_3\text{-OH})(\mu\text{-dmnpz})_3(\text{OCOCH}_3)_2(\text{H}_2\text{O})_3]\cdot\text{H}_2\text{O}\cdot\text{EtOH}$ (1). The oxo-trinuclear complex contains two carboxylates coordinated to two Cu(II) ions. It must be pointed out that among the known compounds that have structure 1 from Scheme 1, there are no studies with pyrazole derivatives dressed with different substituents in the 3, 4 and 5 positions, as we approached here. The compounds of type 1 are interesting for the relative simplicity in the interpretation of magnetic properties, the pyrazolate and $\mu_3\text{-OH}$ bridges determining strong antiferromagnetism [28–30].

Performing the reaction with the same starting materials, but changing the solvent with a more basic one, pyridine, the $[\text{Cu}_6(\mu\text{-OH})_6(\mu\text{-dmnpz})_6(\text{Py})_6]\cdot 6\text{Py}\cdot 2\text{EtOH}$ (2) compound was obtained. The neutral complex belongs to the class of six-membered metal-lacycles, several known analogs being: $([\text{Cu}(\mu\text{-OH})(\mu\text{-R}_1\text{,R}_2\text{-pz})_6])$, $\text{R}_1 = \text{R}_2 = \text{H}$ [19,20],

$R_1 = \text{CH}_3$, $R_2 = \text{H}$ [21], $R_1 = \text{CH}_3$, Py, $R_2 = \text{H}$ [22], $R_1 = \text{CF}_3$, $R_2 = \text{H}$ [23,24]. The six-membered rings with unsubstituted pyrazole ligands adopt a crown structure, with a *cis* arrangement, where the six hydroxyl groups of the metallacycle are pointing towards a focal point on an approximate symmetry axis, while the pyrazoles towards the periphery, the ensemble with, consequently, hydrophilic and hydrophobic domains. For substituted pyrazole, or for higher nuclearities of the metallacycles, the crown structures are sketching a *trans* arrangement with half of the OH groups and half of the pyrazolato ligands oriented on the same side, with respect to the mean plane of the metal-ions ring, while the other subsets of these ligands are placed on the opposite hemisphere.

The triangular fragment is remarkably stable and can be used as a secondary building unit (SBU) in the construction of several coordination polymers [31,32]. We succeed in connecting two SBU via six carboxylate anions to a central copper ion to obtain a heptanuclear compound $[\text{Cu}_7(\mu\text{-OH})_2(\mu\text{-dmnpz})_6(\mu\text{-OCOCH}_3)_6(\text{MeOH})_6]$ (3), in the shape of an hourglass. Enlarging, by future syntheses and analyses, the list of the heptanuclears belonging to the structural type 3 (see Scheme 1) can be proposed as a challenging task.

Our attention was focused on the reaction of copper(II) carboxylates with pyrazole derivatives, 3,5-dimethyl-4-nitro-pyrazole (dmnpz), observing that different nuclearities and topologies depend on the employed solvent. The pyrazole (dmnpz) was synthesized according to Scheme 2 [33–35].



Scheme 2. Synthesis of the used pyrazole ligand.

2. Materials and Methods

2.1. Materials and Physical Measurements

All reagents were of analytical grade, being used without further purification. 3,5-dimethyl-4-nitro-pyrazole (dmnpz) was synthesized according to literature procedures [33–35]. The content in carbon, hydrogen and nitrogen was determined by elemental analysis using a Perkin Elmer PE 2400 analyzer (Perkin Elmer, Boston, MA, USA). The IR spectra were performed by a JASCO 4200 spectrometer with Pike ATR unit in the $400\text{--}4000\text{ cm}^{-1}$ range (JASCO, Tokyo, Japan). The magnetic data were collected in the range of $2\text{--}300\text{ K}$ at an applied field of 0.1 T on a MPMS-5S SQUID magnetometer (Quantum Design, San Diego, CA, USA). The diamagnetism was corrected by Pascal constants [36].

2.2. Synthesis

2.2.1. $[\text{Cu}_3(\mu_3\text{-OH})(\mu\text{-dmnpz})_3(\text{OCOCH}_3)_2(\text{H}_2\text{O})_3]\cdot\text{H}_2\text{O}\cdot\text{EtOH}$ (1)

A solution of copper acetate monohydrate $\text{Cu}(\text{CH}_3\text{COO})_2\cdot\text{H}_2\text{O}$ (0.4 g, 2 mmol) in ethanol/water (5 mL/5 mL) was added drop wise, under continuous stirring, to a solution of dmnpz (0.282 g, 2 mmol) in ethanol (5 mL). The resulting blue-greenish mixture was stirred at room temperature for 24 h and then filtered. A blue microcrystalline precipitate formed, and was subsequently filtered, washed with EtOH and dried under vacuum. It was recrystallized from EtOH, yielding in few days dark greenish-blue crystals for (1), suitable for X-ray crystal structure determination and for all measurements. Yield (based on Cu^{2+}): 73%. Elemental Analysis: calc. for $\text{C}_{21}\text{H}_{39}\text{Cu}_3\text{N}_9\text{O}_{16}$ (Mr = 864.22): C, 29.19; H, 4.55; N, 14.59; Found: C, 28.78; H, 4.42; N, 14.01%. FT-IR (cm^{-1}): 3517(w), 3446(w), 2916(w), 1673(m), 1538(s), 1474(s), 1404(s), 1354 (vs), 1312 (sh), 1171 (s), 1093 (w), 1008 (sh), 980(m), 952(sh), 832(s), 754(m), 599 (w), 486(w), 457(m), 408(w).

2.2.2. $[\text{Cu}_6(\mu\text{-OH})_6(\mu\text{-dmnpz})_6(\text{Py})_6]\cdot 6\text{Py}\cdot 2\text{EtOH}$ (2)

A solution of copper acetate monohydrate $\text{Cu}(\text{CH}_3\text{COO})_2\cdot\text{H}_2\text{O}$ (0.4 g, 2 mmol) in ethanol (5 mL) was added drop wise, under continuous stirring, to the dmnpz solution (0.282 g, 2 mmol) in ethanol (5 mL). The resulting green mixture was stirred at room temperature for 24 h and then filtered. The filtered clear solution was removed and the separated green solid was recrystallized from pyridine. The blue pyridine solution was slowly evaporated in a cooler. Suitable greenish-blue crystals for (2), which appeared in six months, were used for all the measurements. Yield (based on Cu^{2+}): 54%. Elemental Analysis: calc. for $\text{C}_{94}\text{H}_{114}\text{Cu}_6\text{N}_{30}\text{O}_{20}$ ($M_r = 2365.38$): C, 47.73; H, 4.86; N, 17.76. Found: C, 46.63; H, 4.77; N, 16.02%. FT-IR (cm^{-1}): 3382(w), 3177(m), 1595(w), 1538(m), 1474(m), 1439(sh), 1418(s), 1376 (m), 1348 (vs), 1171 (m), 1100 (w), 1029 (w), 987(m), 902(w), 839(m), 768(w), 690 (m), 606 (w), 535(w), 479(w).

2.2.3. $[\text{Cu}_7(\mu\text{-OH})_2(\mu\text{-dmnpz})_6(\mu\text{-OCOCH}_3)_6(\text{MeOH})_6]$ (3)

A solution of copper acetate monohydrate $\text{Cu}(\text{CH}_3\text{COO})_2\cdot\text{H}_2\text{O}$ (0.4 g, 2 mmol) in methanol (5 mL) was added slowly, under stirring, to a dmnpz solution (0.282 g, 2 mmol) and Et_3N (0.202 g, 0.28 mL, 2 mmol) in methanol (15 mL). The resulting green solution was stirred at room temperature for 24h and then filtered. The clear dark green solution was slowly evaporated at room temperature. Suitable green crystals for (3), appeared in few days, and were used for all the instrumental measurements. Yield (based on Cu^{2+}): 89%. Elemental Analysis: calc. for $\text{C}_{48}\text{H}_{80}\text{Cu}_7\text{N}_{18}\text{O}_{32}$ ($M_r = 1866.07$): C, 30.89; H, 4.32; N, 13.76. Found: C, 30.47; H, 4.38; N, 13.14%. FT-IR (cm^{-1}): 3586 (m), 3446(m), 2980(w), 1683(w), 1658(m), 1542(vs), 1521(m), 1472(s), 1457(sh), 1416(vs), 1379 (s), 1357 (vs), 1176 (s), 1108 (w), 1029 (w), 990(m), 835(m), 763(w), 690(m), 606(w), 530(w), 484(w), 419(w).

2.3. X-ray Crystallography

A Rigaku Rapid II R-Axis diffractometer ($\text{MoK}\alpha$ ($\lambda = 0.71075\text{\AA}$), was used to collect the diffraction data of complexes 1–3. All calculations were performed using the Crystal-Structure [37] crystallographic software package. The refinement was performed using the Olex1.2 [38] program. The structure was solved by direct methods and refined in a routine manner (SHELXL) [39]. Non-hydrogen atoms were refined anisotropically. The hydrogen atoms were refined using the riding model. Molecular graphics were generated by MERCURY 3.9 [40] and POV-Ray [41] software. The details of the X-ray crystal data and the structure solutions, as well as the refinements, are given in Table S1. A summary of selected bond lengths (\AA) and angles (in degrees $^\circ$) is outlined in Tables S2–S4 (see Supplementary Materials). The Crystallographic data for the structures reported in this paper have been deposited in the Cambridge Crystallographic Data Centre with CCDC reference numbers 2059160 for compound 1, 2059163 for 2 and 2059182 for 3.

2.4. Computational Methods

The calculations were realized on the experimental geometries of the complex compounds, obtained from the X-ray diffraction analysis, in the frame of Density Functional Theory (DFT) [42], using the B3LYP [43] functional and 6-31G* basis on copper, nitrogen and oxygen, while 6-31G for the carbon and hydrogen atoms [44]. The calculations were done with the GAMESS [45] suite.

3. Results and Discussions

3.1. Structural Analysis from Crystallographic Data

3.1.1. Structure of Compound 1

The asymmetric unit of complex 1 contains two molecular complexes with slight mutual differences and disordered solvent molecules, which affect the final refinement parameters. In Figure 1 we present only one molecular species, the couple of closely similar structures being shown in Supplementary Materials (Figure S1). Each molecule (see Figure 1), $[\text{Cu}_3(\mu_3\text{-OH})(\mu\text{-dmnpz})_3(\text{OCOCH}_3)_2(\text{H}_2\text{O})_3]$, reveals a triangular trinuclear

neutral core. The copper ions are connected via a trihapto oxygen from a central hydroxyl group and three bridging pyrazolate ligands. Two acetate ions are coordinated, each to Cu1 and Cu3 sites. Two water molecules are linked to the Cu2 center and another one to Cu1. The structure of compound **1** is special for containing, simultaneously, three distinct stereochemistries of copper ions, which can be quantified by the help of so-called τ_5 [46] and τ_4 [47] indices. The idealized margins are: $\tau_5 = 0$ for a square-pyramidal complex, while $\tau_5 = 1$ for a trigonal bipyramidal frame; $\tau_4 = 0$ for a square planar unit, while $\tau_4 = 1$ for a tetrahedral case. The sites in compound **1** can be characterized as square pyramid for Cu1 (with $\tau_5 = 0.227$), trigonal bipyramid for Cu2 (with $\tau_5 = 0.567$) and square planar for Cu3 ($\tau_4 = 0.098$).

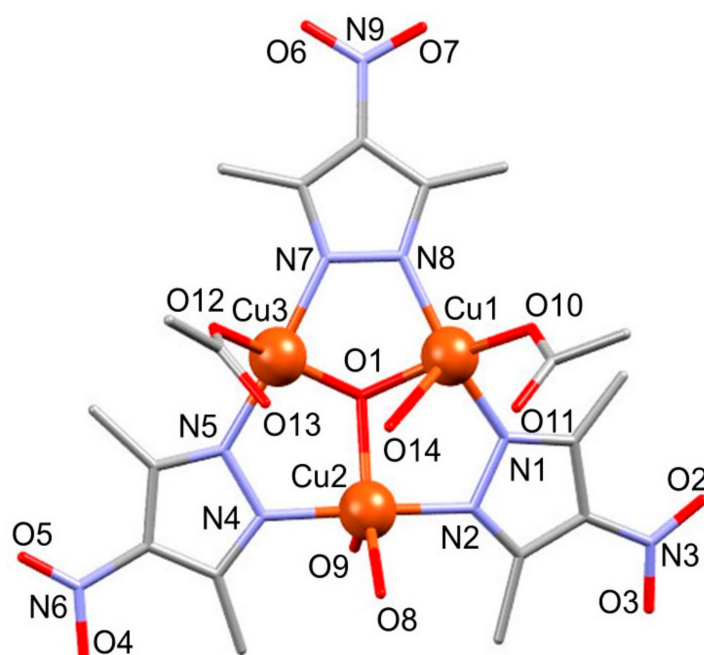


Figure 1. Asymmetric unit of compound **1** with partial atom labeling scheme. Hydrogen atoms are omitted for clarity.

The triangular frame is not symmetric, having different Cu–Cu distances. There are slightly different bond lengths formed by copper and central oxygen (Cu1–O1 1.974(8) Å, Cu2–O1 2.039(8) Å, Cu3–O1 1.985(8) Å), larger than those reported for systems with the same core [48]. The capping μ_3 -O(1)H group is out of the plane formed by copper ions, displaced by about 0.752(2) Å. Two of the Cu–O(H)–Cu angles are very close to each other (Cu1–O1–Cu3 and Cu1–O1–Cu2, 105.7(4)° and 105.0(4)°, respectively), quite different in comparison with the third one (Cu2–O1–Cu3 109.3(4)°). Only one pyrazolate ring bearing N4–N5 is coplanar with the copper ions moiety, since the other two pyrazolate rings (N1–N2 and N7–N8) are displaced out of the {Cu₃} plane, conferring to the overall structure a flattened bowl-shape. The Cu–N(bridged) distances are all in the range of 1.939(13)–1.984(12) Å. The Cu–N–N(bridged) angles are in the 115.1(9)–119.2(9)° interval.

The triangular bowl-shaped molecules are stacked along the *a* axis (Figure 2) within a columnar arrangement established through hydrogen bonds, the most interesting being the hydrogen bond between the carboxylate group coordinated to Cu1 and the O(1)H group from the next molecule (O1'–O11 = 2.738(4) Å). The distance between the copper ion planes in this packing is slightly alternating, by 7.086 and 7.100 Å. The packing details for **1** are presented in Figures S2–S4 from the Supplementary Materials.

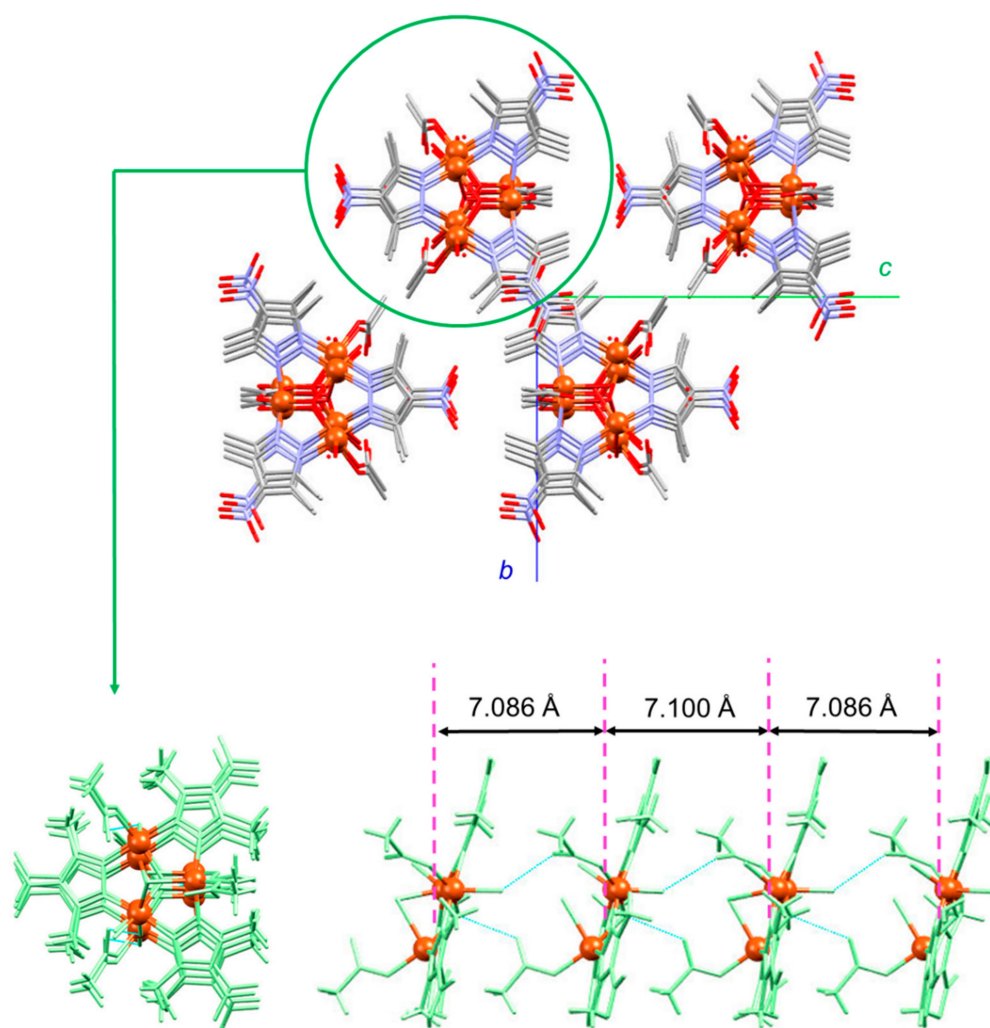


Figure 2. Packing diagram for compound **1** along *a* axis (**top**) and packing detail along *c* axis, showing the supramolecular column arrangement stabilized by hydrogen bonds (**bottom**).

The structural parameters for compound **1** are very poor, due to a severe disorder of two solvent molecules and the poor quality of crystals. Therefore, we consider it as a structural model for the further discussions. However, the reduced resolution, does not imply doubts about the molecular structures themselves. Since compound **1** is important in the red line of this work as preamble to compound **3**, a system with a high degree of novelty, we carry on the discussion, retaining this slight caveat.

3.1.2. Structure of Compound **2**

The compound **2** crystallized in a triclinic system, R-3 space group. As seen in Figure 3, the molecular unit of **2** consists in a six membered metallacycle copper (II) pyrazolate, where the copper atoms are in a hexagonal planar geometry, with a Cu–Cu distance of 3.32 Å. The neutral cyclic complex $[\text{Cu}_6(\mu\text{-OH})_6(\mu\text{-dmnpz})_6(\text{Py})_6]$ contain six distorted square-pyramidal Cu ions with $\tau_5 = 0.44$ stereochemical index [46]. The square pyramide basis plane is formed by two nitrogen atoms from two dmnpz ligands arranged in *trans* (Cu1–N1 = 2.018(4) Å and Cu1–N2 = 2.003(4) Å) and two oxygen atoms from the OH (Cu1–O1 = 1.943(4) Å, Cu1–O1 = 1.947(4) Å) bridging groups. The apical position of each site is occupied by pyridine (Cu1–N4 = 2.359(5) Å). The pyridine molecules are coordinated in the plane of the copper ring, while the dmnpz and OH groups are forming two bowl-shaped cavities. Such cavities can accommodate guest molecules, and in our case, two disordered ethanol molecules are involved. The compound **2** shows a hexagonal tubular structure,

on the packing along *c* axis, which can be interesting for further debate on the porosity properties. The packings for **2** are presented in Supplementary Materials Figures S6–S8.

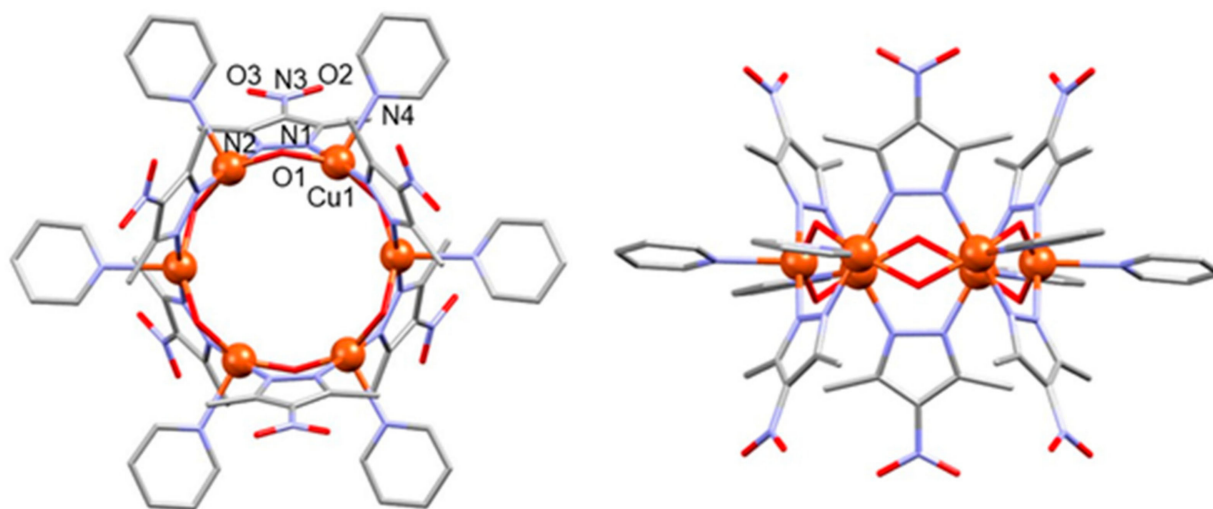


Figure 3. Asymmetric unit of compound **2** with atom numbering scheme (left side). Side-view (right half). Hydrogen atoms and solvent molecules are omitted for clarity.

3.1.3. Structure of Compound **3**

The compound **3** has a surprising symmetry, crystallizing in the trigonal system, *R*- $\bar{3}c$ space group. The structure (Figure 4) shows an “hourglass” pattern with two trinuclear triangular copper complexes at the ends, connected to a central octahedral copper ion via carboxylate anions coordinated in chelating and bridging fashion. The compound can be viewed like consisting of two oxo-trinuclear units, which act here like SBUs.

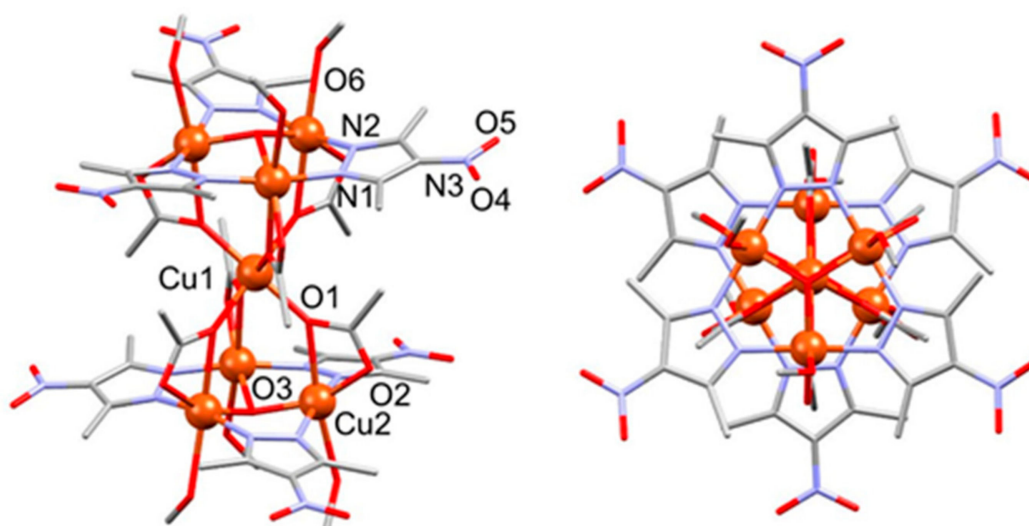


Figure 4. Asymmetric unit of compound **3** with atom numbering scheme (left). Side-view (right). Hydrogen atoms are omitted for clarity.

The three-fold axis is oriented along O3, O3A and the central Cu1 atom. The copper ions from the trinuclear SBU have an elongated octahedral geometry, along the O1–Cu2–O6 direction with 2.462(4) and 2.506 Å bond lengths, respectively. The current literature knows two similar compounds, one with the same ligand, reported by Lang and Zhu [24], following a single crystal-to-single-crystal transformation, where ligated-EtOH molecules were

replaced with MeOH. The mentioned authors did not carry further investigations, while the interesting pattern deserves detailed attention, as we devoted in the following. According to the Cambridge Structural Database, there is a second compound with the same pattern (CCDC 853959, refcod XEMYIZ), including a different pyrazole derivative, respective 3,5-bis-(trifluoromethyl)-pyrazole [25]. This last study includes only the structural analysis.

A synopsis of the discussed structures, highlighting for view and measurements the copper atoms, is given in Figure 5. As advocated previously and proved by the following analyses, the considered structural patterns have prototypic virtues. The conclusions extracted from specific structural analyses show generalized relevance for all the previous and future members of each class. The next section, devoted to the formal spin coupling models, comprises useful methodological advances, extracting new closed formulas, usable for the simulation of the magnetic properties of the considered prototypes.

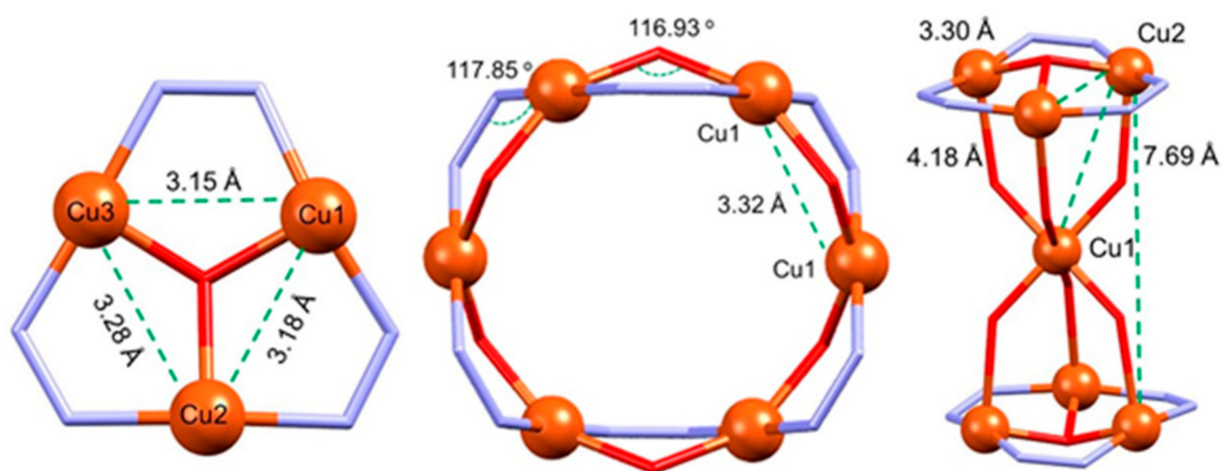


Figure 5. The structural patterns and Cu–Cu distances of the compounds **1** (left side), **2** (center) and **3** (right side).

3.2. Spin Hamiltonians and Magnetic Data

3.2.1. Spin Hamiltonian and Magnetic Susceptibility Equations

In the following, we will rely on the Heisenberg-Dirac-van Vleck (HDvV) Spin Hamiltonian [49,50],

$$\hat{H}_{HDvV} = -2 \sum_{j < i} J_{ij} \hat{S}_i \cdot \hat{S}_j \quad (1)$$

for accounting for the magnetic properties of the discussed systems. The general treatment of large or non-symmetric systems demands the full numeric approach, namely constructing and resolving Hamiltonian matrices having the dimension of the total number of spin states, taken as the product of local spin multiplicities on the constituent ions. In the case of copper homo-metallic systems with nuclearity N , the total number of states (including the $2S + 1$ spin degeneracies) is 2^N . In the absence of further spin-type interactions (like Zeeman, dipolar, spin-orbit or zero-field-splitting), the whole matrices are factorized in blocks corresponding to total spin projections, S_z , and furthermore by total spin quantum numbers, S , provided that the corresponding basis transformations are made. Solving the Hamiltonian as eigenvectors E_I , associated to total spin quantum numbers S_I , the product between magnetic susceptibility and temperature is given by the van Vleck equation [36]:

$$(\chi T)_{HDvV} = \frac{N_A \beta^2}{3k_B} \cdot \frac{\sum_I g_I^2 \cdot S_I(S_I + 1)(2S_I + 1) \cdot \text{Exp}\left(-\frac{E_I}{k_B T}\right)}{\sum_I (2S_I + 1) \cdot \text{Exp}\left(-\frac{E_I}{k_B T}\right)} \quad (2)$$

where N_A and k_B are Avogadro and Boltzmann constants, β is the Bohr magneton and g_I are gyromagnetic factors of each state, algebraically formed from g_i parameters of each

paramagnetic center. Often, a global unique g^2 factor is taken, which is literally true in the case of equivalent isotropic sites. Sometimes, the practice imposes adding certain empirical correction terms, such as the linear add-on,

$$\chi T = (\chi T)_{HDvV} + PIM + TIP \cdot T \quad (3)$$

with a constant off-set having the meaning of paramagnetic impurity (PIM) and the slope known as temperature independent paramagnetism (TIP) [36]. The paramagnetic impurity can come literally from inherent sample conditions, or can cumulate extended lattice interactions, not accounted by the assumed molecular model. The TIP can result from first order expansion of non-HDvV interactions, such as spin-orbit or dipolar terms, being then a surrogate avoiding higher, possibly unreachable, complexity of the case.

The general procedure for numerical handling of the HDvV Hamiltonian in its matrix representation can be tedious and have a black box nature. Fortunately, the discussed systems can be presented in a transparent fashion, as it follows. Thus, we will draw explicit formulas for the counted E_I states of the systems, as a function of involved HDvV coupling parameters and the defining spin quantum numbers.

3.2.2. The Magnetism of the Trinuclear Complex

The trinuclear compound has three pyrazoles as bridges, having the appearance of an almost isosceles triangle. The slightly different coordination sites make the exchange couplings on the Cu–Cu edges inequivalent, while yet comparable. The case of a general triangle (scalene), with all edges inequivalent, is tractable by closed energy formulas. Putting the lowest spin doublet in the energy origin, we have the following relative spin state energies for the two spin-doublet states and quartet:

$$E\left(S = \frac{1}{2}\right)_1 = 0 \quad (4)$$

$$E\left(S = \frac{1}{2}\right)_2 = 2\sqrt{J_{12}^2 + J_{13}^2 + J_{23}^2 - J_{12}J_{13} - J_{12}J_{23} - J_{13}J_{23}} \quad (5)$$

$$E\left(S = \frac{3}{2}\right) = -J_{12} - J_{13} - J_{23} + \sqrt{J_{12}^2 + J_{13}^2 + J_{23}^2 - J_{12}J_{13} - J_{12}J_{23} - J_{13}J_{23}} \quad (6)$$

However, on the existing data, the general model cannot safely discriminate three different couplings. As the calculations described in the following indicate, the different coupling values are comparable, so that one may go on the simplified hypothesis of equal parameters: $J = J_{12} = J_{13} = J_{23}$. In this case, one may benefit from the simplified formula, as a function of the total spin quantum number:

$$E(S) = -JS(S + 1) \quad (7)$$

One may easily verify that shifting the $E(S = 1/2)$ from Equation (7) to zero, the equilateral triangle is obtained as a particular situation of the above ascribed (4–5) formulas for a scalene topology. The above result is very well-known, belonging to the class of so-called Kambe formulas [51,52]. However, for the sake of completeness, let us recall here the derivation. The spin Hamiltonian of the equilateral triangle is:

$$\hat{H}_{M_3} = -2J(\hat{S}_1 \cdot \hat{S}_2 + \hat{S}_1 \cdot \hat{S}_3 + \hat{S}_2 \cdot \hat{S}_3) \quad (8)$$

Then, observe that the operator can be rewritten as follows:

$$2(\hat{S}_1 \cdot \hat{S}_2 + \hat{S}_1 \cdot \hat{S}_3 + \hat{S}_2 \cdot \hat{S}_3) = (\hat{S}_1 + \hat{S}_2 + \hat{S}_3)^2 - \hat{S}_1^2 - \hat{S}_2^2 - \hat{S}_3^2 = S(S + 1) - S_1(S_1 + 1) - S_2(S_2 + 1) - S_3(S_3 + 1) \quad (9)$$

The last equality involves the regularity that the sum of local spin operators yields the total spin operator, \hat{S} , and the \hat{S}^2 quantum square is $S(S + 1)$, in all instances of total or local spins. Since the sum comprising the square of the three local spin operators is a constant shift, it can be eliminated, arriving at Equation (9). In the regular triangle, the two $S = 1/2$ levels are degenerate, in a multiplet with “e” orbital label in the D_{3h} symmetry. Then, this is a case of the Jahn–Teller effect [53,54], namely experiencing the trend to remove the degeneracy by distorting the molecular frame. Probably this is the reason for which the compound forms itself with slightly inequivalent coordination sites. Considering that the rather rigid pyrazole bridges would not easily allow a sensible distortion of the triangle itself, for example, to an isosceles, the formation of different coordination sites is the alternative, instead of distorting a system having identical coordination sites.

A reasoning succeeding to extract analytic energy formulas from the spin Hamiltonian, linear in all the coupling parameters, is possible in a limited number of cases, with high formal symmetries. Fortunately, one may further exploit such a strategy aiming to describe long the long-range lattice interaction between two equilateral trimers, needed to better account for the magnetism of compound **1**. In this view, we are going to enforce the assumption that all the centers of a trimer are coupled by the same parameter, j , with all the nodes of the other triangle. This is not the realistic situation, but it allows, in the Gordian knot-alike strategy, to tackle the problem in a yet acceptable semiquantitative manner. The idea is that, in this way, one may account for a sort of global interaction between molecular units, as monolithic spin carriers. Then, the Hamiltonian for a dimer of trimers is ascribed as follows:

$$\hat{H}_{M_3-M_3} = -2J(\hat{S}_1 \cdot \hat{S}_2 + \hat{S}_1 \cdot \hat{S}_3 + \hat{S}_2 \cdot \hat{S}_3) - 2J(\hat{S}_4 \cdot \hat{S}_5 + \hat{S}_4 \cdot \hat{S}_6 + \hat{S}_5 \cdot \hat{S}_6) - 2j(\hat{S}_1 \cdot \hat{S}_4 + \hat{S}_1 \cdot \hat{S}_5 + \hat{S}_1 \cdot \hat{S}_6 + \hat{S}_2 \cdot \hat{S}_4 + \hat{S}_2 \cdot \hat{S}_5 + \hat{S}_2 \cdot \hat{S}_6 + \hat{S}_3 \cdot \hat{S}_4 + \hat{S}_3 \cdot \hat{S}_5 + \hat{S}_3 \cdot \hat{S}_6) \quad (10)$$

Let us define the spin operators on molecular moieties:

$$\hat{S}_{123} = \hat{S}_1 + \hat{S}_2 + \hat{S}_3 \quad (11)$$

$$\hat{S}_{456} = \hat{S}_4 + \hat{S}_5 + \hat{S}_6 \quad (12)$$

The total spin is, obviously:

$$\hat{S} = \hat{S}_{123} + \hat{S}_{456} \quad (13)$$

Let us observe that the parenthesis factored by the long-range $-2j$ interaction is actually $\hat{S}_{123} \cdot \hat{S}_{345}$, the scalar product of the spins on individual triangles:

$$\hat{H}_{M_3-M_3} = -2J(\hat{S}_1 \cdot \hat{S}_2 + \hat{S}_1 \cdot \hat{S}_3 + \hat{S}_2 \cdot \hat{S}_3 + \hat{S}_4 \cdot \hat{S}_5 + \hat{S}_4 \cdot \hat{S}_6 + \hat{S}_5 \cdot \hat{S}_6) - 2j\hat{S}_{123} \cdot \hat{S}_{345} \quad (14)$$

Then, using the trick exemplified previously, we can rewrite the Hamiltonian

$$\hat{H}_{M_3-M_3} = -J(\hat{S}_{123}^2 + \hat{S}_{456}^2) - J \sum_{i=1}^6 \hat{S}_i^2 - j(\hat{S}^2 - \hat{S}_{123}^2 - \hat{S}_{456}^2) \quad (15)$$

Dropping the middle constant term (from the summation on local spins and converting the squared operators to their quantum expectation value), one may arrive to a nice simple formula, as a function of the total spin and of spin states on the triangular moieties:

$$E(S, S_{123}, S_{456}) = -(J - j)(S_{123}(S_{123} + 1) + S_{456}(S_{456} + 1)) - jS(S + 1) \quad (16)$$

Then, to concretely apply these formulas, the triads of (S, S_{123}, S_{456}) quantum numbers must be counted properly. For instance, let us exemplify the arising of five global singlet states expected in a system with six $1/2$ local spins. Thus, we have three $S = 0$ states originating from the interaction of each spin state on a trimer with its mirror image on the other one. In addition, two more singlets must be added coming from the cross-coupling of the first singlet at one triangle with the second singlet on the companion, and vice-versa.

The groundstate of the ensemble is expected to formally originate from antiferromagnetic coupling of the lowest doublets on each triangular moiety. Since the first and second doublets are degenerate in the case of the imposed equilateral triangle, the groundstate has a fourfold degeneracy. This is an artificial situation, determined by the rather strong idealization assumed at the beginning. However, in spite of limitations, the transparency enabled by this treatment is quite precious. To the best of our knowledge, such a rationalization was not presented before. The magnetism of stacked trinuclear copper complexes resembling the discussed system is a problem with a certain degree of generality, given the many similar known complexes [10,28,29,55–61], so that the here proposed model acquires a quite relevant meaning.

The dimer of trimers is needed to account for, in an effective manner, the sudden drop of the χT at low temperature, observed in Figure 6. The slow increase of χT in the high temperature domain, without reaching the paramagnetic plateau, is the signature of strong antiferromagnetic coupling. Indeed, we fitted the value $J = -110 \text{ cm}^{-1}$, for the averaged coupling inside the trimer units, altogether with a $g = 2.1$ Landé factor. The global intermolecular parameter was found slightly antiferromagnetic, $j = -3 \text{ cm}^{-1}$. We avoided introducing a TIP correction, although it may seem necessary, considering that, without this, a small plateau trend may appear at intermediate temperatures, till the on-set of a molecular effective magnetic moment, after reaching the saturation of the intermolecular coupling. However, a paramagnetic impurity correction seemed necessary to describe why the χT does not drop nearby zero at the lowest T point, taking then $\text{PIM} = 0.1 \text{ cm}^3 \text{ mol}^{-1} \text{ K}^{-1}$, as an empiric adjustment. The HDvV part was equated with the energies from Equation (16), introduced in the van Vleck master formula (Equation (2)). The resulted $(\chi T)_{\text{HDvV}}$ for the model hexanuclear was divided into a half, to consider the molecular susceptibility of the trimer itself. The concrete enumeration of states and expressions of energy levels are shown in Table S5 of the Supplementary Materials.

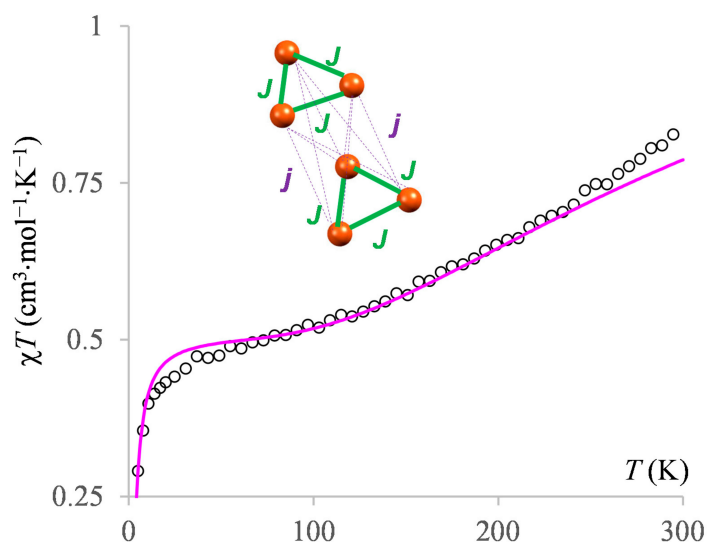


Figure 6. The χT vs. T curve for the trinuclear compound **1**: experimental data (open circles) and fit to model (continuous line). The model is made for the hexanuclear formed as dimer of trimers (shown as sketched inset), in order to account long-range interaction by the unique j coupling parameter, while the χT is taken as a half from the hexamer amount, in order to effectively describe the trimer only.

3.2.3. The Magnetism of the Hexanuclear Complex

The hexamer has a $\{\text{Cu}_6\text{O}_6\}$ ring resembling the chain conformation of the cyclohexane, with the hydroxo-bridges at vertices and the copper ions in the middle of the almost linear O-Cu-O edges. Then, the $\{\text{Cu}_6\}$ subsystem forms a regular planar hexagon. With this note, one may properly say that, from the perspective of exchange coupling effects, the hexanuclear is absolutely similar to the benzene, treated in the frame of a valence bond

theory [62], to which the HDvV effective Hamiltonian is explicitly adequate [63]. From this perspective, one may also speculate that the regular shape of the whole system, with identical coordination spheres of the monomeric units and regular $\{\text{Cu}_6\}$ frame, is a direct consequence of the aromatic-alike stabilization ensured by the exchange interaction in such a topology.

The associated spin Hamiltonian, considering the idealized D_{6h} symmetry, is obvious:

$$\hat{H}_{M_6(D_{6h})} = -2J(\hat{S}_1 \cdot \hat{S}_2 + \hat{S}_2 \cdot \hat{S}_3 + \hat{S}_3 \cdot \hat{S}_4 + \hat{S}_4 \cdot \hat{S}_5 + \hat{S}_5 \cdot \hat{S}_6 + \hat{S}_1 \cdot \hat{S}_6) \quad (17)$$

The hexagonal hexanuclear does not benefit from a simplified Kambe-like tractability. However, taking as a single significant parameter the coupling J along the proximal copper sites, via hydroxo and pyrazolate bridges, the energy levels can be defined explicitly in a numeric manner, as illustrated in Table S6 from the Supplementary Materials. The neglecting of distant interaction within the ring, between copper ions mutually placed in *meta* and *para* is reasonable, considering the very strong antiferromagnetic coupling along the edges (i.e., between *ortho*-type neighbors).

The fit (see Figure 7) demands empirical adjustment with paramagnetic impurity, since the χT values are not dropping to zero at low temperatures, as expected from the antiferromagnetic six-spins system and also a TIP term, to account for a slope in the interval to about 100K, instead of the plateau expected due to large absolute value of the coupling. As will be debated later on, the large coupling is expected from computational hints and also from precedent reported data on comparable systems [64]. We obtained the following fit parameters: $g = 2.1$, $J = -310 \text{ cm}^{-1}$, $\text{PIM} = 0.08 \text{ cm}^3 \text{ mol}^{-1} \text{ K}^{-1}$, $\text{TIP} = 0.00011 \text{ cm}^3 \text{ mol}^{-1} \text{ K}^{-2}$. The above cited work obtained an even larger antiferromagnetic coupling, $J = 650 \text{ cm}^{-1}$. The larger absolute value can be correlated with shorter Cu–Cu distance in the previously reported system, about 3.07 \AA , in comparison with our spacing, at 3.32 \AA . Probably, the positive sign reported by cited authors is a printing error, since according to their data and discussion, the system is recognized as antiferromagnetic, while using the same spin Hamiltonian as in Equation (17). The mentioned work [64] used the Magpack code for fit [65]. Since here we are making explicit the energy levels (see Supplementary Materials, Table S6), we bring further insight to the particularities of hexagonal six-spins systems.

Let us come back to aromaticity-like spin coupling effects [66,67]. Within the HDvV spin Hamiltonian, the resonance energy is $E_{res} = 1.1055 |J|$ [68,69]. Then, with the above fitted coupling value, one obtains $E_{res} = 342.7 \text{ cm}^{-1}$, i.e., about 26.7 kcal/mol. This is an amount that may count in the balance of deciding the stereochemistry of coordination ensembles. Looking at the larger picture, one may conclude the virtues of the HDvV spin Hamiltonian. It can answer to bonding regime problems (see Reference [1] pp. 325–331 and 411–423), being more valuable than a tool for interpreting the magnetism, as is perceived by its intensive use in magnetochemistry. It can account for other chemical species as well, for instance, the aromatic hydrocarbons with spin [70]. On the other hand, as proven here, it can describe certain bonding aspects in coordination compounds, not only their magnetism.

3.2.4. The Magnetism of the Heptanuclear Complex

The heptanuclear compound can be described as a trigonal antiprism having in center another metal ion. The coordination of the central ion is a trigonally distorted octahedron, while the caps of the embedding antiprism resemble the above-discussed trinuclears, having the same $\{\text{Cu}_3(\text{pyrazole})_3\}$ bridged sub-structure.

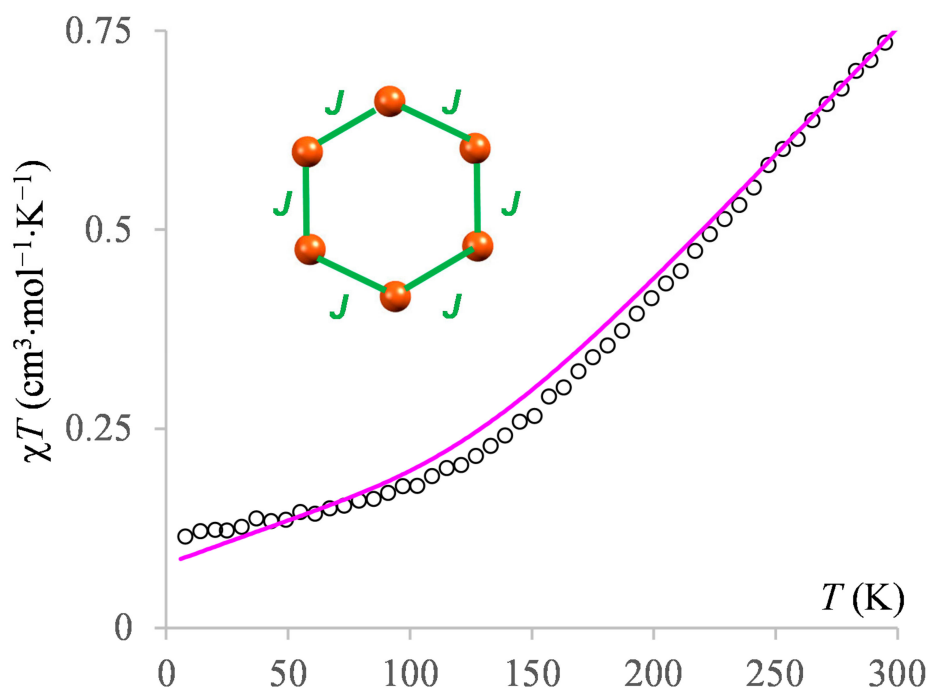


Figure 7. The χT vs. T curve for the hexanuclear compound **2**: experimental data (open circles) and fit to model (continuous line). The model follows the hexagonal pattern, with a J coupling parameter along edges, as illustrated in the inset.

A convenient fact is that the heptamer can be described, in idealized mode, by analytical formulas of the spin of Hamiltonian, provided that the hexamer moiety is taken in a topology as those previously stated and the coupling from the central atom toward all the others is assumed equal, say by the unique parameter J' . Thus, with the M' as the seventh paramagnetic site, having the spin S_7 , while S_{1-6} denotes the quantum number of the hexamer unit, the spin Hamiltonian of the heptamer is defined by the following addition to the hexamer formula:

$$\hat{H}_{M_3-M_3-M'} = \hat{H}_{M_3-M_3} - 2J'\hat{S}_{1-6} \cdot \hat{S}_7 \quad (18)$$

Then, with the total spin S running from $|S_{1-6} - S_7|$ to $S_{1-6} + S_7$, by transformations resembling the previous ones, one arrives at the following formula of the energy levels:

$$E(S, S_{1-6}, S_{123}, S_{456}) = -(J - j)(S_{123}(S_{123} + 1) + S_{456}(S_{456} + 1)) - (j - J')S_{1-6}(S_{1-6} + 1) - J'S(S + 1), \quad (19)$$

indexed with the intermediate spins S_{1-6} , S_{123} and S_{456} .

The magnetic data are shown in Figure 8. Although formally kept, inherited from previous derivation, the j parameter will be ignored, to avoid overcharging the fit. Then, the result is: $g = 2.0$, $J = -130 \text{ cm}^{-1}$, $\text{PIM} = 0.05 \text{ cm}^3 \text{ mol}^{-1} \text{ K}^{-1}$, $\text{TIP} = 0.0001 \text{ cm}^3 \text{ mol}^{-1} \text{ K}^{-2}$. To the best of our knowledge, there are no other literature data on similar compounds to be compared with.

The Supplementary Materials contains in Table S7 details on the spin states in the copper heptanuclear.

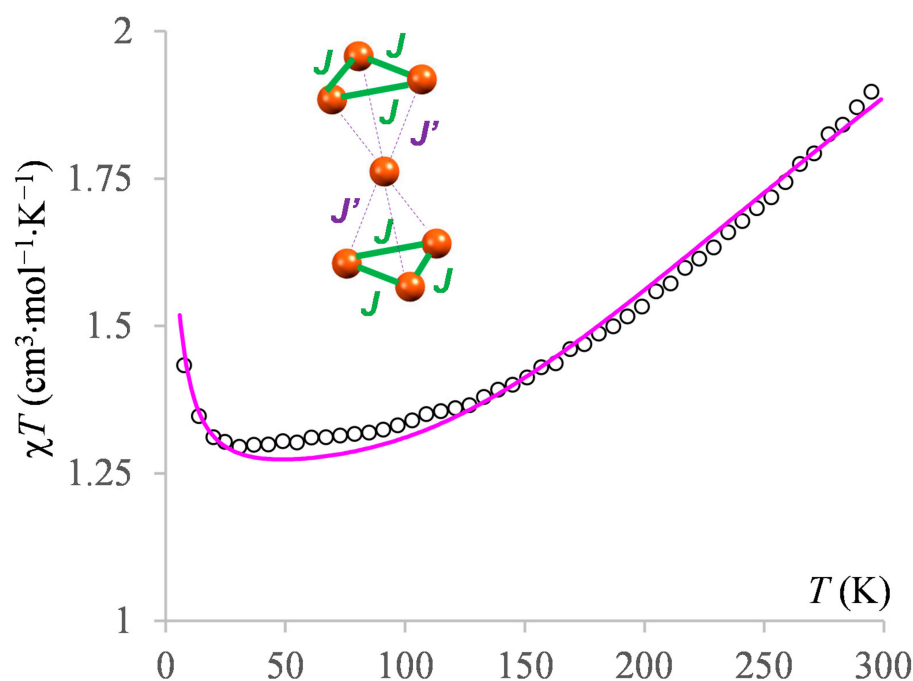
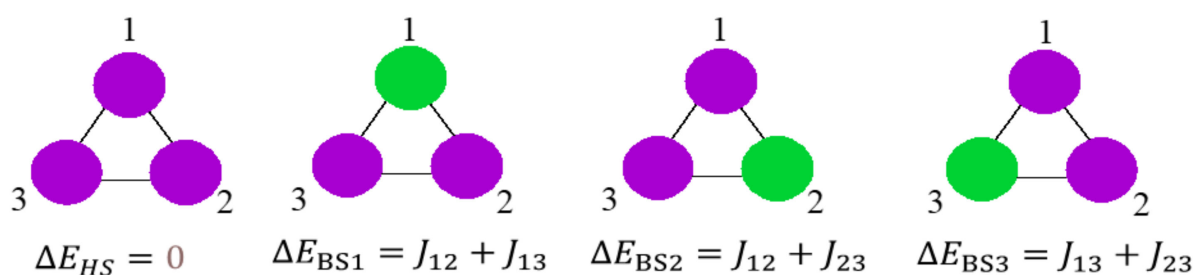


Figure 8. The χT vs. T curve for the heptanuclear compound **3**: experimental data (open circles) and fit to model (continuous line). The model consists of merging the above-defined dimer of trimers, based on J, j couplings with a central node having equivalent parameters, J' towards the vertices of the hexamer. At the end, the j parameter is neglected, imposing $j = 0$ in the actual fit. The inset annotates the considered J and J' interactions.

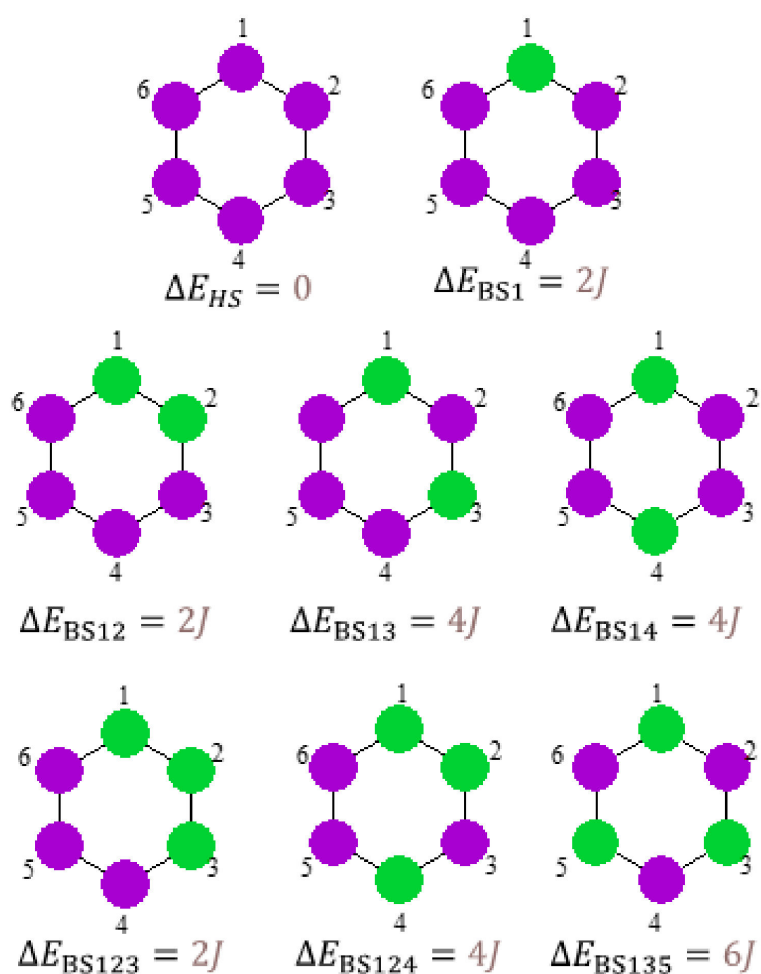
3.3. Broken Symmetry (BS) Calculations

3.3.1. Realization and Interpretation of BS Calculations

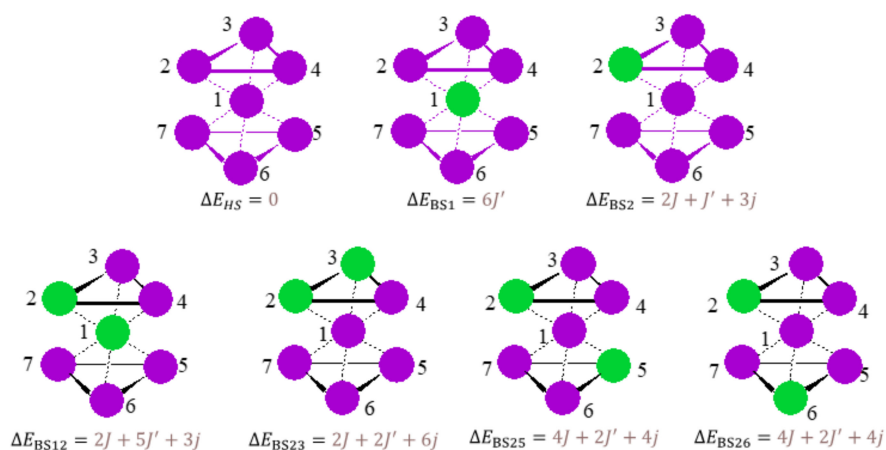
The so-called Broken Symmetry (BS) approach [71–74] represents the strategy usable to obtain estimations of exchange coupling parameters in the frame of Density Functional Theory. The BS-DFT calculations in compounds with many metal centers are laborious, since they are implying the obtaining of single-determinants with unrestricted localized orbitals, having a controlled spin polarization distribution on specific centers. Namely, they must drive the convergence toward defined maps, switching, by proper educated guesses, the local spin population on coordination sites between α or β preponderance. In this view, we proceeded by the following steps: (i) first, do the unrestricted calculation of the system with highest spin multiplicity (HS); (ii) collect the natural orbitals, emulating in this way a restricted-type result; (iii) perform an orbital localization, focusing on functions having singly-occupied nature; (iv) duplicate the sequences of restricted-type localized orbitals, as the initial guess for both α and β unrestricted subsets; (v) initiate the desired number of BS calculations operating the corresponding permutations in α and β orbital lists, in order to achieve the intended spin-flip scheme. The following Schemes 3–5 should be regarded as a roadmap for the desired sequence of HS and BS calculations, customized by the described algorithm, while the subsequent Figures 8–14, with spin density maps, can be seen as a confirmation for achieving the targeted patterns.



Scheme 3. The qualitative patterns of spin polarization (α in purple, β in green) and corresponding model energies for Broken Symmetry (BS) configurations in a trinuclear system.



Scheme 4. The qualitative spin polarization patterns (α in purple, β in green) and model energies for symmetry-independent position isomers of BS configurations in a regular hexagon.



Scheme 5. The spin polarization patterns (α in purple, β in green) and model energies for symmetry-independent position isomers of BS states compound 3. The $S_z = 1/2$ states are omitted.

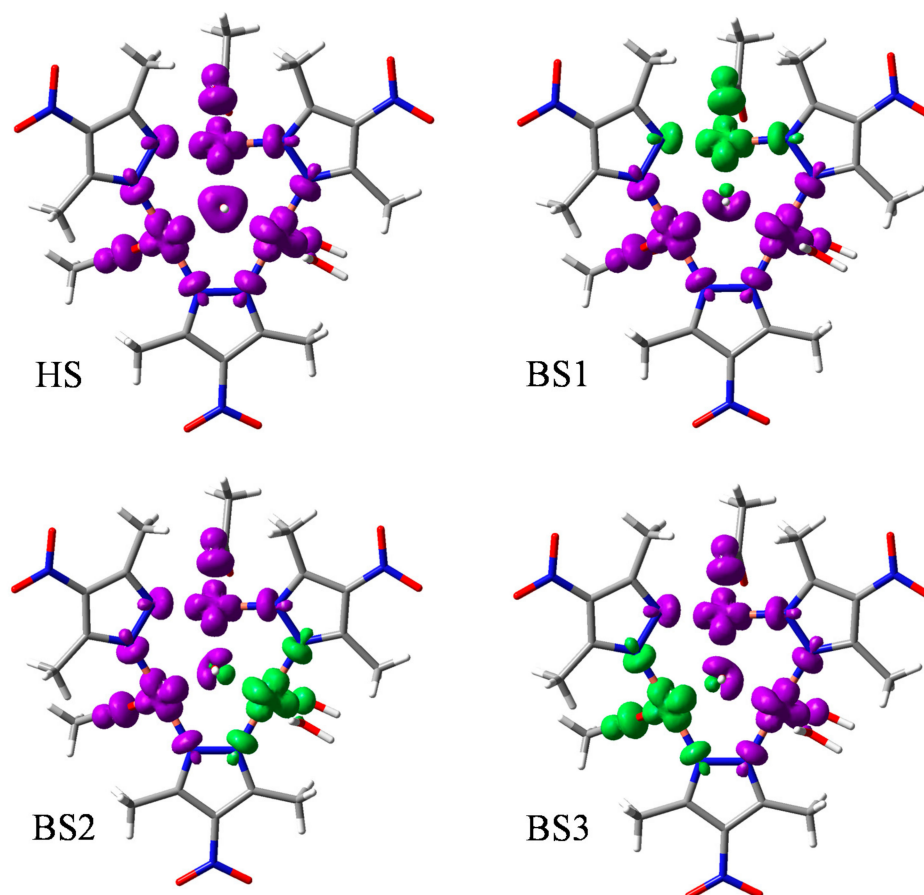


Figure 9. The spin density maps of the unrestricted density functional theory (DFT) calculations for the highest spin (HS) and BS configurations for the trinuclear unit of compound 1, drawn at $0.05 \text{ e}/\text{\AA}^3$ isosurfaces. The violet and green colors are representing the α and β spin densities, respectively. Note that the spin swap occurs on the aimed centers, as sketched in green in Scheme 3.

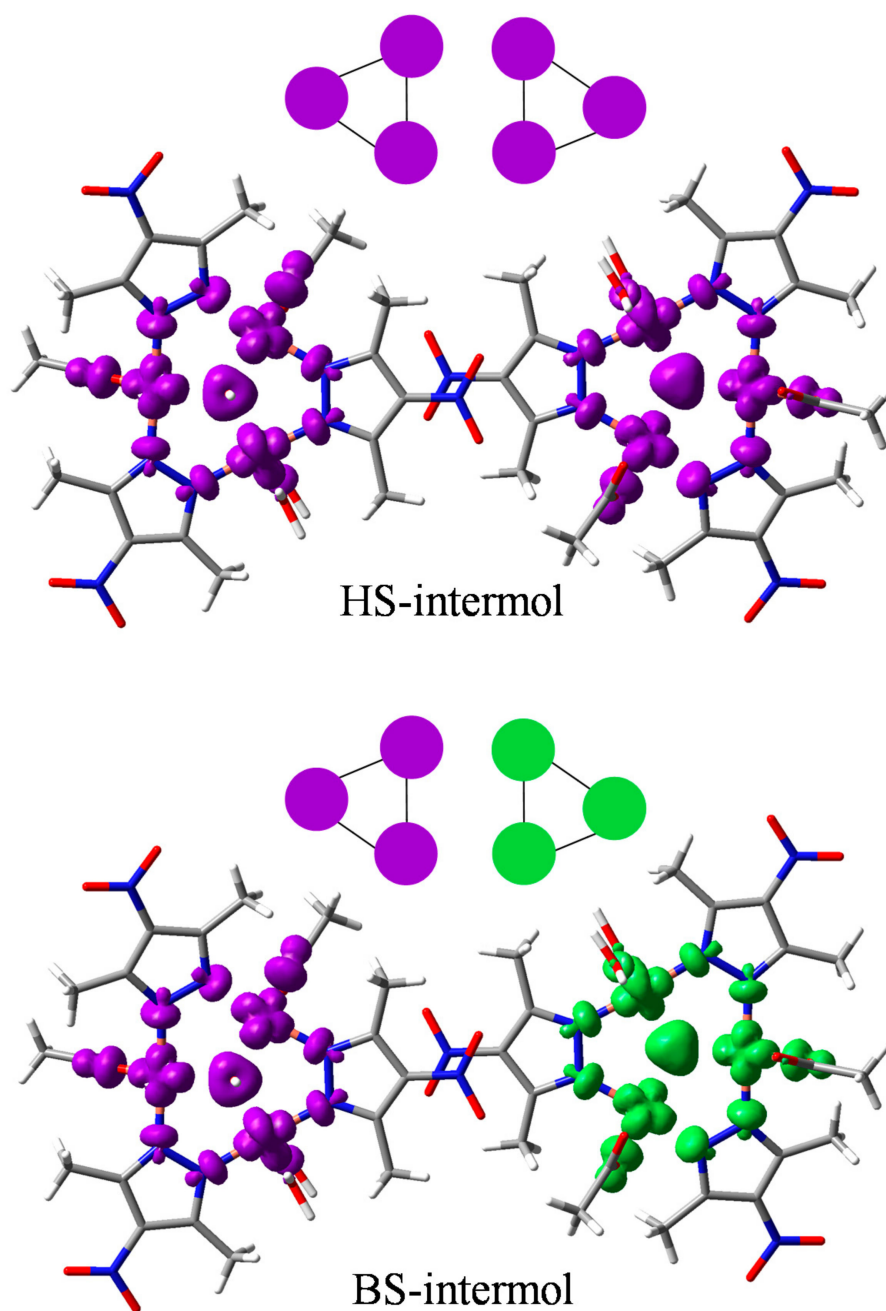


Figure 10. The spin density maps for the BS calculations attempting the description of the intermolecular spin coupling. The couple of dimers is taken as an excerpt from the crystal structure. The qualitative schemes are shown as insets.

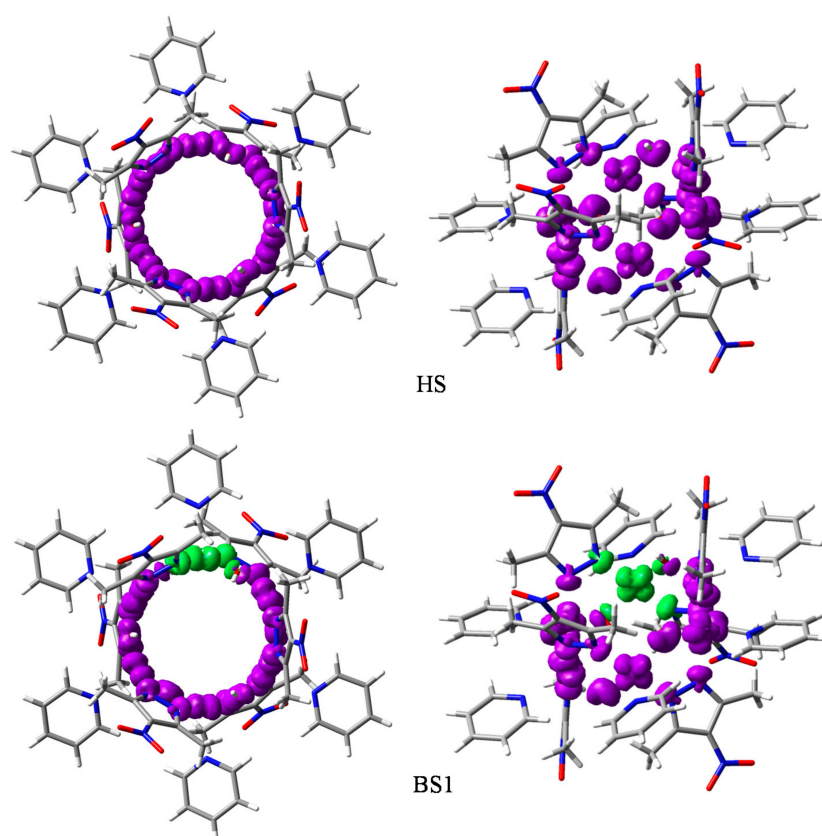


Figure 11. The spin density maps for the HS (**upper** half) and BS1 (**lower** half) for the copper hexamer. The isosurfaces are drawn at the $0.05 \text{ e}/\text{\AA}^3$ threshold. The violet and green colors represent the α and β spin densities, respectively.

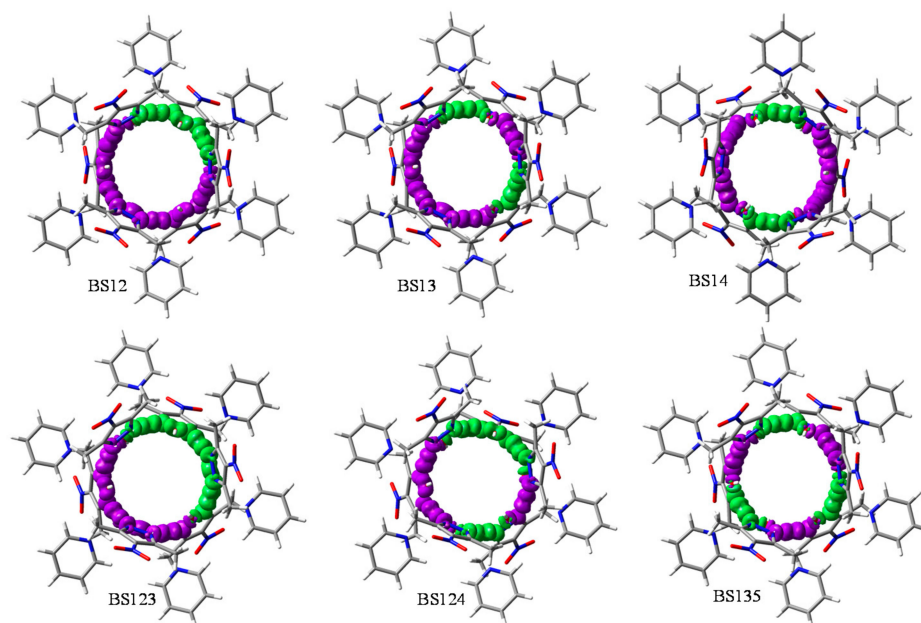


Figure 12. The spin density maps for the BS configurations with $S_z = 1$ (**upper** half) and $S_z = 0$ (**lower** half) for the copper hexamer. The isosurface coloring and drawing threshold is the same as in Figure 9. Note that the green zones are matching the patterns planed in Scheme 4.

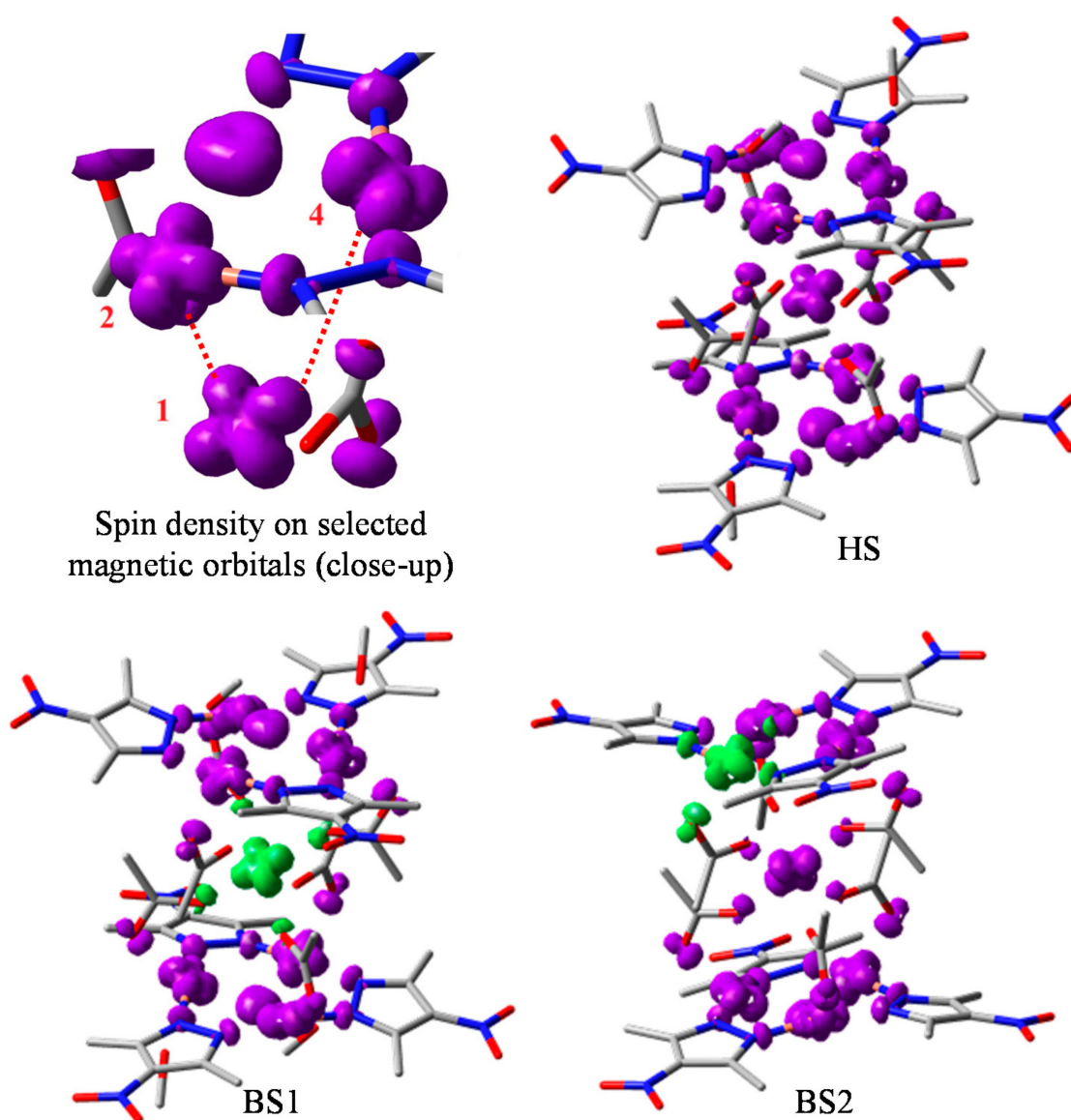


Figure 13. The spin density maps for the $S_z = 7/2$ (HS) and $S_z = 5/2$ (BS1, BS2) configurations of the heptanuclear complex, drawn at $0.01 \text{ e}/\text{\AA}^3$ isosurfaces. The upper-left corner shows a magnification from the HS spin density map, emphasizing the d-type profiles on the metal ions labeled 1, 2 and 4. A part of the structure components (metal center #3 and certain ligand fragments) were erased to ease the visibility to the portions suggesting the mutual orientation of the magnetic orbitals.

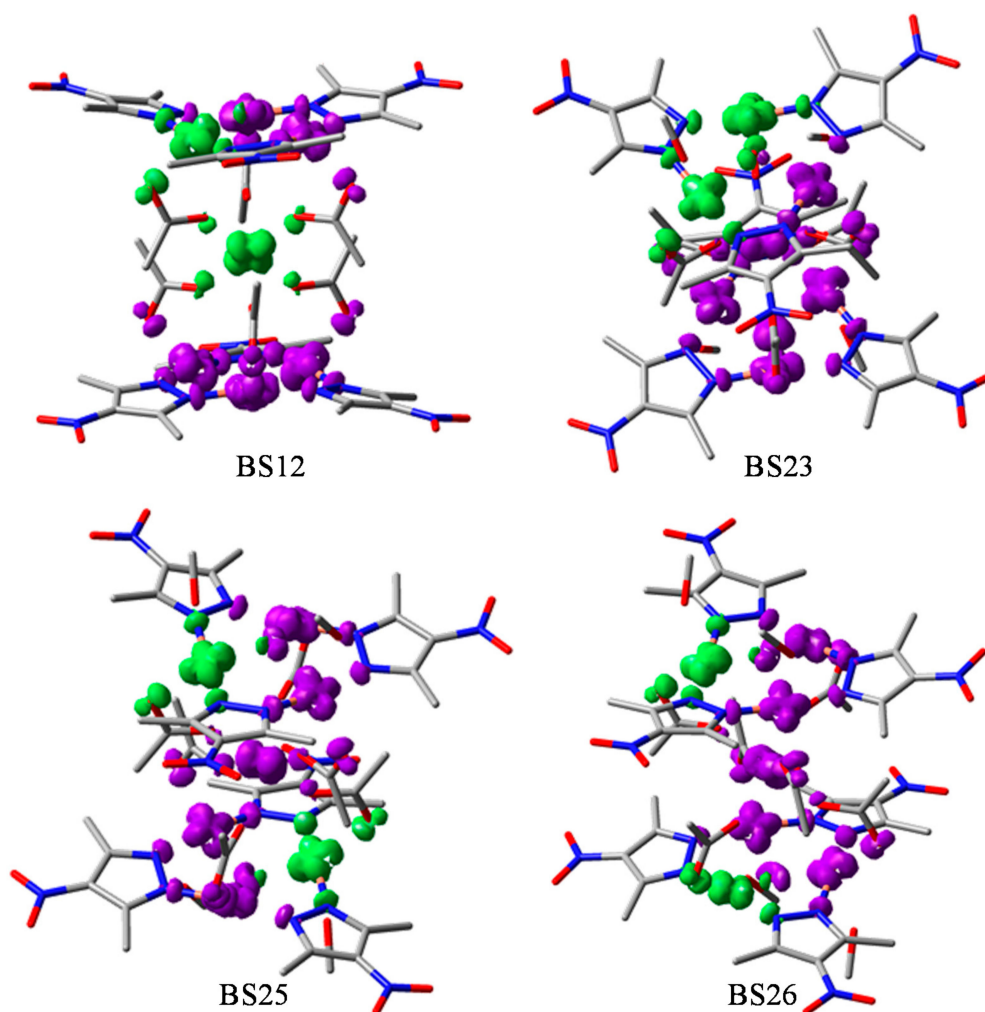


Figure 14. The spin density maps for the $S_z = 5/2$ (BS12, BS23, BS25 and BS26) configurations of the heptanuclear complex, drawn at $0.01 \text{ e}/\text{\AA}^3$ isosurfaces. Molecular frames are slightly rotated, mutually, in order to ensure better visibility of the sites with β spin density (green surfaces). A part of the half-coordinated methanol molecules was removed to clear the visibility of density surfaces.

The interpretation of BS calculations is straightforward in binuclear systems, the case of higher polynuclears being debated by Shoji et al. [75]. We also outlined a general procedure, exposed in Reference [1] pp. 629–633. Other methodological considerations for equating BS in polynuclears were advanced by Ruiz [76].

The easiest way for interpretation is to directly rely on the so-called Ising spin Hamiltonian, to which the BS calculations are conceptually related. For the sake of clarity, we will try to reformulate now, in a simple way, the handling of BS data in polynuclears, given the chance of the panoply of systems presented here as a quite interesting application. The Ising form takes simple numeric products of spin projections instead of scalar products of true spin operators, met in Equation (1):

$$\hat{H}_{\text{Ising}} = -2 \sum_{j < i} J_{ij} S_i^z S_j^z \quad (20)$$

By convention, the above formula can be taken without the -2 factor in the front of the summation. The Ising Hamiltonian is invoked in certain dedicated physical problems where pseudospins are adopted as the conventional description of certain site properties [77,78], but actually is of little use in the molecular magnetism itself. The Ising-type expression is nothing else than the form of the diagonal elements in the matrix formulation

of the full HDvV Hamiltonian. Therefore, the Ising energies are not directly usable in a physical problem, but it happens that these are parallel to the meaning of energy in BS configurations [76].

The BS treatments imply achieving calculations that reverse the local spin site from projection $S_i^z = +S_i$ to $S_i^z = -S_i$, starting from the reference with all spins up. Note that the whole spin population of a given site should undergo the transmutation from α to β local density, intermediate projections not being admitted as of BS nature. In the case of sites with one unpaired electron, i.e., $S_i = 1/2$, as are our copper polynuclears, the only possibilities are, of course, $S_i^z = \pm 1/2$.

In a practical sense, we shall rely on the BS energies relative to those of the highest spin. The high spin (HS) configuration has the following Ising energy:

$$E_{HS} = -2 \sum_{j < i} J_{ij} S_i S_j \quad (21)$$

A BS configuration, labeled ω , can be ascribed as consisting in a sequence of spin-flip factors, $\sigma_{ij} = \pm 1$, as follows:

$$E_{BS(\omega)} = -2 \sum_{j < i} \sigma_{ij}(\omega) J_{ij} S_i S_j \quad (22)$$

Obviously, we have $\sigma_{ij} = 1$ for projections with the same sign, ($S_i^z > 0$ and $S_j^z > 0$) or ($S_i^z < 0$ and $S_j^z < 0$), and $\sigma_{ij} = -1$ in the case of opposite projections. Let us take the difference between a given BS state, ω , and the HS reference:

$$\Delta E_{BS(\omega)} = E_{BS(\omega)} - E_{HS} = -2 \sum_{j < i} (\sigma_{ij}(\omega) - 1) J_{ij} S_i S_j \quad (23)$$

In a simplified recipe, the summation on pairs, $j < i$, retains only the terms with $\sigma_{ij} = -1$, i.e., the situations where a relative spin flip occurs at the given i - j contact. The Ising-like interpretation results can be saliently applied (using the DFT computed energies of the different BS(ω) configurations) as long as the corresponding computed expectation values of the squared spin, $\langle S(S+1) \rangle_\omega$, are well retrieving the following regularity:

$$\Delta \langle S(S+1) \rangle_\omega = \langle S(S+1) \rangle_\omega - \langle S(S+1) \rangle_{HS} = -2 \sum_{j < i} (\sigma_{ij}(\omega) - 1) S_i S_j \quad (24)$$

All the computations presented in the following are obeying this demand. Note that, while Equation (23) can omit the ij couples for which J_{ij} is assumed negligible, the summation in Equation (24) should include all the possible pairs. For details, see Reference [1] pp. 629–633.

3.3.2. The BS Calculations of the Trinuclear Complex

The BS treatment of a triangle with inequivalent edges implies one HS configuration with $S_z = 3/2$ total spin projection and three configurations with $S_z = 1/2$, labeled BS*i*, according to the address of the i center lodging the β spin. These are qualitatively represented in Scheme 3, according to the explicit $\Delta E(\text{BS}i)$ general formulas. The computed BS energies of states, relative to the HS, are -287.6 , -259.2 and -257.0 cm^{-1} , at the reversal of the spin on the respective coordination sites labeled 1, 2 and 3. With the model equations ascribed in Scheme 3, one may deduce the following distinct coupling parameters, $J_{12} = -144.9 \text{ cm}^{-1}$, $J_{13} = -142.7 \text{ cm}^{-1}$ and $J_{23} = -114.3 \text{ cm}^{-1}$.

As initially guessed from qualitative structural considerations, these parameters are mutually comparable, indebted the approximate treatment as equilateral. In the regular triangle, the energy of each BS state is $2J$, the computed average being $J = -134.0 \text{ cm}^{-1}$. This result is in good relation with the above-reported fit value (see Section 3.2.4). The

differences in spin-squared expectation values, $\Delta\langle S(S+1)\rangle_{\text{HS}} - \Delta\langle S(S+1)\rangle_{\text{BS}}$ are, in all three cases, about 2.03, i.e., close to the ideal quantity, namely 2.

The spin density maps of HS and BS configurations are revealing the shapes of the magnetic orbitals carried by each site (see Figure 9). Obviously, the sign information associated to the wave-function lobes is lost in such representations, having only the orbital contours. Thus, one may observe the “four leaf clover” shapes corresponding to the d-type orbitals and mushroom-like profiles of the lone pairs from pyrazole and acetate ligands. The central oxygen has a donut shape in the HS map, being affected by spin polarization in the BS cases, when it forms asymmetric lobes. One observes that the BS spin reversal is spreading also on the neighboring ligands, which are also colored in green around the β d-type orbital. The four-lobe d-type orbitals are oriented almost in the Cu(pyrazole) local frames, certifying that the N-Cu-N axes are those undergoing the strongest ligand field. Slight tilts out of the $\{\text{Cu}_3\}$ plane seem to be determined by the pyramidalization of the coordinated central hydroxo group above the copper triangle fragment. If we define the local coordination axes with x along the N-Cu-N average directions and y along the Cu-O linkages toward the central group, then the magnetic orbitals of each coordination site can be named qualitatively as $x^2 - y^2$. Details on the BS-DFT data of the presented system are in Table S8 from the Supplementary Materials.

Subsequently, we tried to investigate in the BS methodology the intermolecular interaction, roughly described by the j parameter in the model from Section 3.2.2. As discussed, the j factorizes the interaction between the whole trimer moieties. We considered a pair of molecules as a model which, in crystal are related almost by an inversion center (corresponding to Figure S1 in Supplementary Materials). The BS treatment can be simply realized taking one trimer moiety in the HS configuration, while another one has the same appearance, reverted in β spin density, as illustrated in Figure 10. Although the BS intermolecular spin coupling regime is achieved, as certified by the obtained spin density maps (see Figure 10), the energy difference between the HS and BS forms is practically null. In turn, the fit discussed in Section 3.2.2 found a small, yet sizeable, intermolecular antiferromagnetism. There may be multiple reasons for the computational failure. First of all, one may suspect the intrinsic drawbacks of current density functionals in describing long-range effects [79,80]. We refrained from introducing any of the many possible empirical long-range corrections [81–84], since none of these were calibrated for such subtle goals. Another possibility stays in the limitation of the “dimer of trimers” model. In the crystal, such supramolecular contacts are continued as chains and sheets. Then, a very small coupling at a dimeric sequence can be amplified, in the band structure interaction regime, to a sizeable coupling effect. Thus, the fitted j , formally assigned to a dimer, actually describes effects from extended systems. Since the failures are also a part of the fair scientific inquires, we mentioned the case here.

3.3.3. The BS Calculations of the Hexanuclear Complex

The BS calculations on the hexagonal complex are challenging, facing the situation of many position isomers in terms of mutual placement of the α and β sites. Since only one coupling parameter must be found, J , a single BS configuration will suffice. However, treating the whole set implies a challenging technical virtuosity, and besides, retrieving the same J value will certify the validity of the BS approach itself.

Scheme 4 outlines in a qualitative manner the distinct symmetry BS states possible in a regular hexagon. The labeling by BS_i , BS_{ij} and BS_{ijk} denotes the i , j or k sites taking the β spin in the respective situations when one, two or three spin swaps are made with respect to the HS state (with $S_z = 3$ spin projection). There is only one distinct isomer with $S_z = 2$ projection, marked as BS1 (equivalent with one spin reversed on any center). The $S_z = 1$ has the three possibilities of *ortho*-, *meta*- and *para*- BS isomers, labeled BS12, BS13 and BS14, respectively. Finally, the $S_z = 0$ has the BS123, BS124 and BS135 cases. Their energies, relative to the HS are printed in Scheme 4. There is a simple recipe to retrieve the BS formulas: the cofactor of a given type of J is the count of edges carrying circles of

different colors, in the drawn insets of Scheme 4. Details on the BS-DFT data of the hexamer are in given Table S9 from the Supplementary Materials.

In order to extract information about the shape of magnetic orbitals, Figure 11 shows the HS and BS1 configurations, each, in two orientations. One view is perpendicular to the mean plane of the metal ions ring, aiming to verify the obtaining, from computation, of the spin polarization pattern charted in Scheme 4. The views presented on the left side of Figure 11 are allowing to view the sites labeled 1 and 4 particularly. Thus, one may observe the four-lobed orbitals oriented perpendicularly to the Cu_6 plane. The lone pairs due to pyrazole ligands have mushroom shapes. The spin delocalized over a hydroxo bridge takes the hearth-like shapes in the HS maps and in the points bridging ions with the same spin. As a bridge between different local spin projections, the OH groups are polarized in two-lobe profiles, with different colors. Interestingly, as a bridge between two spin projections, the pyrazoles get one lone pair colored in purple and one in green, certifying the inner spin polarization. Figure 12 shows the top view of the other computed BS spin density maps.

The relative BS energies for the {BS1, BS12, BS13, BS123, BS124, BS135} sequence are, correspondingly, {−480.6, −482.0, −960.2, −961.0, −481.9, −961.5 and −1439.0} (values in cm^{-1}). Dividing these quantities by coefficients of J ascribed in Scheme 4 as analytic BS energies, the following estimations for the J parameters are, respectively, obtained: {−240.3, −241.0, −240.1, −240.3, −241.0, −240.4 and −239.8} (all values in cm^{-1}). Thus, all the estimations from the different BS calculations are very close to the $J = -240 \text{ cm}^{-1}$, the whole treatment being validated. The value is reasonably close, in semiquantitative respects, to the J resulted from fit, in Section 3.2.3.

3.3.4. The BS Calculations of the Heptanuclear Complex

The heptamer presents a very large number of BS position isomers, whether the whole set is aimed. We will limit ourselves to the configurations with the following definitions: $S_z = 7/2$ (HS), $S_z = 5/2$ (BS1 and BS2, as symmetry distinct species) and $S_z = 3/2$ (BS12, BS23, BS25 and BS26). Thus, we eluded the case of smallest projection, $S_z = 1/2$, with a large number of positional mutations. The full BS-DFT data are posted in Table S10 from Supplementary Materials. The considered set of six configurations offers sufficient information to extract the three parameters assumed by the model presented in Section 3.2.4, namely J for coupling inside the triangular caps of the structure, J' , for all the contacts between these faces and the central atom, and j for the presumably weak effects between triangular faces. The BS configurations and their model energies are presented in Scheme 5. One may observe again the simple recipe for the BS formulas, by summing all the coupling parameters picked from edges encountering centers of opposed spin polarity. This simple rule, based on Ising interpretation is valid if the check assumed by Equation (24) is approximately passed. Thus, the ideal values for the $\langle S(S+1) \rangle_{\text{HS}} - \langle S(S+1) \rangle_{\text{BS}}$ differences are 6 and 10 for the respective $S_z = 5/2$ and $S_z = 3/2$ subsets. The computational details given in Table S7 from Supplementary Materials are illustrating that this regularity is held with reasonable accuracy, within the second decimal digit.

The relative energies for the (BS1, BS2, BS12, BS23, BS25 and BS26) sequences are {27.7, −313.9, −294.3, −312.0, −631.8 and −643.8}, respectively (all values in cm^{-1}). The least square solutions of the BS equations are: $J = -162.3 \text{ cm}^{-1}$, $J' = +4.9 \text{ cm}^{-1}$, $j = +0.75 \text{ cm}^{-1}$. One may remark that the J coupling corresponds to a strong antiferromagnetism, while the J' is weakly ferromagnetic, in line with the experimental data. The magnitudes of the computed parameters are matching the range of the experimental ones. Somewhat intriguingly, the computed j coupling results as ferromagnetic, too. This parameter was not the object of the fit and is difficult to charge the problem with too many parameters, because of the inherent uncertainties, given the rather large parametric list.

A further detailing of the issue can be reached associated to the BS fit, complicating the model a bit. Thus, relaxing the constraint of a unique coupling parameter inside the hexanuclear subunit, one may propose two sorts of long-range interactions: a j_c , corre-

sponding to the sites placed mutually in *cis*, inside the trigonally distorted octahedron and a j_t , for the *trans* couples. With this detailing, the BS25 and BS26 become inequivalent, the $4j$ term becoming $4j_c$ and $2j_c + 2j_t$, respectively. Within the new BS model fit, the following values are found $J = -163.0 \text{ cm}^{-1}$, $J' = +5.0 \text{ cm}^{-1}$, $j_c = +2.8 \text{ cm}^{-1}$ and $j_t = -2.7 \text{ cm}^{-1}$.

Aside from verifying the success of BS attempts, by retrieving in the computed spin density maps the patterns envisaged at the beginning of calculations, according to the chart form Scheme 5, Figures 13 and 14 are offering information about implied magnetic orbitals. Particularly, it is relevant to observe the magnified excerpt from the upper-left corner of Figure 13, showing the d-type profiles for the central atom (#1) and for two atoms from the upper triangle (#2 and #4). One notes that the four-lobe profile of the atom #1 is tilted by about 45° with respect to the planes of the two Cu_3 moieties. Inside the trimeric fragments, the four-lobe shapes are approximately perpendicular to the axes formally connecting the given sites to the central atom, being therefore tilted with about 30° from their Cu_3 planes. Looking along the dashed line drawn between #1 and #2 copper sites (see the upper-left corner of Figure 13) one may say that, if this is taken as the z axis in a local coordinate frame, then the corresponding magnetic orbitals look like a $x^2 - y^2$ and a xy couple. Then, falling in a sort of orthogonality relationship (null overlap), one may guess that this coupling is prone to ferromagnetic nature, according to the basic paradigms of magneto-structural correlations [85–88]. Also, an almost-orthogonality can be proposed for the contact along the #1–#4 line, having the situation of the first site with one lobe approximately aligned to this axis (behaving then as able for σ -type bonding), while the other metal-based orbital has the lobes roughly perpendicular to the intercentrum direction (as if ready for δ -type overlap). The orbital interaction along the #1–#3 line follows a similar situation. By symmetry, the interaction between the central magnetic orbital and those of the other face undergo a mirroring of mutual overlap relations. Then, the orbital quasi-orthogonality reasons are explaining the ferromagnetic coupling between the central atom and the embedding cluster, obtained from fit and computational simulations.

4. Conclusions

The work deals with the structural chemistry of a series of newly synthesized coordination polynuclear compounds, seen from multiple perspectives, experimental, theoretical and in correlation with the magnetic properties. The common feature of the presented systems is the functionality of pyrazolate bridges as reinforcement of molecular edifices.

The clusters sketched by the Cu(II) centers show remarkable patterns: almost equilateral triangles, regular hexagon and centered trigonal antiprism, for the respective tri-, hexa- and heptanuclears. Remarkably, the last two systems span high space group symmetries, R-3 and R-3c. The opportunity of meeting iconic patterns allows naming the compounds 1, 2 and 3 as representative for the described distinct topologies. In this way, the methods and outcomes related to their structural analyses show general relevance, extended upon past and future relatives falling in the 1, 2 or 3 classes.

Whether the actual literature knows many analogs of 1 and several congeners of 2, compound 3 has only two previously reported relatives, lacking detailed insight. The fact that compound 3 uses the 1-type subsystems as a starting base affords the prediction that this class can be further grown by systematic synthetic attempts.

The presented compounds occasioned new Kambe-type systematization of energy levels, namely having analytical formulas, linear in terms of existing coupling parameters. Whether the equilateral triangle is a well-known Kambe case, we extended this treatment for two interacting trimers, the model being usable for the effective account of long-range effects in the class of compound 1. We also found Kambe-like formulas for system 3. The hexagon from case 2 does not admit Kambe rationalization, but we considered explicit numeric expression for the energy levels, making its treatment transparent. Remarkably, system 2 can be legitimately presented as a case of coordination polynuclear aromaticity. To the best of our knowledge, such developments related with the spin Hamiltonian methodologies were not presented previously.

The excursion is concluded with the simulation of exchange coupling parameters through BS-DFT calculations (Broken Symmetry). The BS approach consists of numeric experiments aiming at the controlled swap of spin polarization on designated centers. At relatively high nuclearities (as 6 or 7), the BS approach is non-trivial, in the technical respect, demanding proper educated guesses of the orbitals used to initiate the calculations.

The interpretation of BS computational results is somewhat challenging, outlining here clear and simple recipes. The presented systems show, as a distinct signature, the strong antiferromagnetic coupling along the pyrazolate bridges. The spin density maps of various BS position isomers (different symmetry-distinct ways to switch from α to β the site spin, at one or many centers) are certifying the success of the attempted BS configurations. The spin density maps are enabling the view of site-specific magnetic orbitals.

Supplementary Materials: The following are available online at <https://www.mdpi.com/2624-8549/3/1/31/s1>, Figure S1: X-ray molecular structure of compound **1** with atoms coloring scheme, Figures S2–S4: Packing along a , b and c axes for compound **1**, Figure S5: X-ray molecular structure of compound **2** with atoms coloring scheme, Figures S6–S8: Packing along a , b and c axes for compound **2**, Figure S9: X-ray molecular structure of compound **3** with atoms coloring scheme, Figures S10 and S11: Packing along a , b and c axes for compound **3**, Table S1: Crystal data for complexes **1–3**, Table S2: Selected bond lengths [Å] and angles [°] for **1**, Table S3: Selected bond lengths [Å] and angles [°] for **2**, Table S4: Selected bond lengths [Å] and angles [°] for **3**, Table S5: The count and energies of spin states (including total and intermediate spin quantum numbers) in a copper hexanuclear system, constituted as dimer of trimers, with the topology discussed in the main text, Table S6: Numeric energies in a hexanuclear system with local 1/2 spin centers and hexagonal topology (having unique exchange coupling parameter J along the edges), Table S7: The count and energies of spin states in a copper heptanuclear system, constituted as a central atom interacting equivalently with two trimers, Tables S8–S10: The high spin (HS) and broken symmetry (BS) energies calculated for compounds **1–3**.

Author Contributions: Conceptualization, supervision, writing—review and editing, validation, F.C. and M.F.; methodology, software, F.C.; formal analysis, data curation, A.-I.T.; data curation, visualization, investigation, original draft preparation, A.M.T. and M.C.B.; resources, C.M.Z. and L.O.C.; funding acquisition, L.O.C. and M.F. All authors have read and agreed to the published version of the manuscript.

Funding: This research and the APC were partially funded by a grant from the Romanian Ministry of Education and Research, CCCDI-UEFISCDI, project number PN-III-P2-2.1-PED-2019-3009, within PNCDI III and University of Bucharest.

Institutional Review Board Statement: Not applicable.

Conflicts of Interest: The authors declare no conflict of interest.

References

1. Putz, M.V.; Cimpoesu, F.; Ferbinteanu, M. *Structural Chemistry, Principles, Methods, and Case Studies*; Springer: Cham, Switzerland, 2018; pp. 629–633. [[CrossRef](#)]
2. Thompson, L.K. Polynuclear coordination complexes – from dinuclear to nonanuclear and beyond. *Coord. Chem. Rev.* **2002**, *233–234*, 193–206. [[CrossRef](#)]
3. Halcrow, M.A. Pyrazoles and pyrazolides-flexible synthons in self-assembly. *Dalton Trans.* **2009**, 2059–2073. [[CrossRef](#)] [[PubMed](#)]
4. Mukherjee, R. Coordination chemistry with pyrazole-based chelating ligands: Molecular structural aspects. *Coord. Chem. Rev.* **2000**, *203*, 151–218. [[CrossRef](#)]
5. Solomon, E.I.; Sundaram, U.M.; Machonkin, T.E. Multicopper Oxidases and Oxygenases. *Chem. Rev.* **1996**, *96*, 2563–2606. [[CrossRef](#)]
6. Cole, A.P.; Root, D.E.; Mukherjee, P.; Solomon, E.I.; Stack, T.D. A trinuclear intermediate in the copper-mediated reduction of O₂: Four electrons from three coppers. *Science* **1996**, *273*, 1848–1850. [[CrossRef](#)]
7. Kaim, W.; Rall, J. Copper—A “Modern” Bioelement. *Angew. Chem. Int. Ed.* **1996**, *35*, 43–60. [[CrossRef](#)]
8. Lee, S.K.; George, S.D.; Antholine, W.E.; Hedman, B.; Hodgson, K.O.; Solomon, E.I. Nature of the intermediate formed in the reduction of O₂ to H₂O at the trinuclear copper cluster active site in native laccase. *J. Am. Chem. Soc.* **2002**, *124*, 6180–6193. [[CrossRef](#)]
9. Tsukerblat, B.S.; Kuyavskaya, B.Y.; Belinskii, M.I.; Ablov, A.V.; Novotortsev, V.M.; Kalinnikov, V.T. Antisymmetric Exchange in the Trinuclear Clusters of Copper (II). *Theor. Chim. Acta* **1975**, *38*, 131–138. [[CrossRef](#)]

10. Ferrer, S.; Lloret, F.; Bertomeu, I.; Alzuet, G.; Borrás, J.; Garcya-Granda, S.; Liu-Gonzalez, M.; Haasnoot, J.G. Cyclic Trinuclear and Chain of Cyclic Trinuclear Copper(II) Complexes Containing a Pyramidal $\text{Cu}_3\text{O}(\text{H})$ Core. Crystal Structures and Magnetic Properties of $[\text{Cu}_3(\mu_3\text{-OH})(\text{aaat})_3(\text{H}_2\text{O})_3](\text{NO}_3)_2 \cdot \text{H}_2\text{O}$ [aaat = 3-Acetylamino-5-amino-1,2,4-triazolate] and $[\{\text{Cu}_3(\mu_3\text{-OH})(\text{aat})_3(\mu_3\text{-SO}_4)\} \cdot 6\text{H}_2\text{O}]_n$ [aat = 3-Acetylamino-1,2,4-triazolate]: New Cases of Spin-Frustrated Systems. *Inorg. Chem.* **2002**, *41*, 5821–5830. [[CrossRef](#)]
11. Rudra, I.; Wu, Q.; Voorhis, T.V. Predicting exchange coupling constants in frustrated molecular magnets using density functional theory. *Inorg. Chem.* **2007**, *46*, 10539–10548. [[CrossRef](#)]
12. Wang, L.; Sun, Y.; Yu, Z.; Qi, Z.; Liu, C. Theoretical investigation on trigonal symmetry copper trimers: Magneto-structural correlation and spin frustration. *J. Phys. Chem. A* **2009**, *113*, 10534–10539. [[CrossRef](#)] [[PubMed](#)]
13. Yoon, J.; Solomon, E.I. Ground-state electronic and magnetic properties of a μ_3 -Oxo-bridged trinuclear Cu(II) complex: Correlation to the native intermediate of the multicopper oxidases. *Inorg. Chem.* **2005**, *44*, 8076–8086. [[CrossRef](#)] [[PubMed](#)]
14. Afrati, T.; Dendrinou-Samara, C.; Raptopoulou, C.; Terzis, A.; Tangoulis, V.; Tshipis, A.; Kessissoglou, D.P. Experimental and theoretical study of the antisymmetric magnetic behavior of copper inverse-9-metallacrown-3 compounds. *Inorg. Chem.* **2008**, *47*, 7545–7555. [[CrossRef](#)] [[PubMed](#)]
15. Canon-Mancisidor, W.; Spodine, E.; Paredes-Garcia, V.; Venegas-Yazigi, D. Theoretical description of the magnetic properties of μ_3 -hydroxo bridged trinuclear copper(II) complexes. *J. Mol. Model.* **2013**, *19*, 2835–2844. [[CrossRef](#)]
16. Angaroni, M.; Ardizzoia, G.A.; Beringhelli, T.; La Monica, G.; Gatteschi, D.; Masciocchi, N.; Moret, M. Oxidation reaction of $[\{\text{Cu}(\text{Hpz})_2\text{Cl}\}_2](\text{Hpz} = \text{pyrazole})$: Synthesis of the trinuclear copper(II) hydroxo complexes $[\text{Cu}_3(\text{OH})(\text{pz})_3(\text{Hpz})_2\text{Cl}_2] \cdot \text{sol}$ (sol = H_2O or tetrahydrofuran). Formation, magnetic properties, and X-ray crystal structure of $[\text{Cu}_3(\text{OH})(\text{pz})_3(\text{py})_2\text{Cl}_2] \cdot \text{py}$ (py = pyridine). *J. Chem. Soc. Dalton Trans.* **1990**, 3305–3309. [[CrossRef](#)]
17. Sakai, K.; Yamada, Y.; Tsubomura, T.; Yabuki, M.; Yamaguchi, M. Synthesis, Crystal Structure, and Solution Properties of a Hexacopper (II) Complex with Bridging Hydroxides, Pyrazolates, and Nitrates. *Inorg. Chem.* **1996**, *35*, 542–544. [[CrossRef](#)]
18. Angaridis, P.A.; Baran, R.; Boča, R.; Cervantes-Lee, F.; Haase, W.; Mezei, G.; Raptis, R.G.; Werner, R. Synthesis and Structural Characterization of Trinuclear Cu^{II} – Pyrazolato Complexes Containing $\mu_3\text{-OH}$, $\mu_3\text{-O}$, and $\mu_3\text{-Cl}$ Ligands. Magnetic Susceptibility Study of $[\text{PPN}]_2[(\mu_3\text{-O})\text{Cu}_3(\mu\text{-pz})_3\text{Cl}_3]$. *Inorg. Chem.* **2002**, *41*, 2219–2228. [[CrossRef](#)]
19. Mezei, G.; Baran, P.; Raptis, R.G. Anion Encapsulation by Neutral Supramolecular Assemblies of Cyclic Cu^{II} Complexes: A Series of Five Polymerization Isomers, $[\{\text{cis-Cu}^{\text{II}}(\mu\text{-OH})(\mu\text{-pz})\}_n]$, $n=6, 8, 9, 12$, and 14 . *Angew. Chem. Int. Ed.* **2004**, *43*, 574–577. [[CrossRef](#)]
20. Fernando, I.R.; Surmann, S.A.; Urech, A.A.; Poulsen, A.M.; Mezei, G. Selective total encapsulation of the sulfate anion by neutral nano-jars. *Chem. Commun.* **2012**, *48*, 6860–6862. [[CrossRef](#)]
21. Canon-Mancisidor, W.; Gomez-Garcia, C.J.; Espallargas, G.M.; Vega, A.; Spodine, E.; Venegas-Yazigi, D.; Coronado, E. Structural re-arrangement in two hexanuclear Cu^{II} complexes: From a spin frustrated trigonal prism to a strongly coupled antiferromagnetic soluble ring complex with a porous tubular structure. *Chem. Sci.* **2014**, *5*, 324–332. [[CrossRef](#)]
22. Henkelis, J.J.; Jones, L.F.; de Miranda, M.P.; Kilner, C.A.; Halcrow, M.A. Two Heptacopper(II) Disk Complexes with a $[\text{Cu}_7(\mu_3\text{-OH})_4(\mu\text{-OR})_2]^{8+}$ Core. *Inorg. Chem.* **2010**, *49*, 11127–11132. [[CrossRef](#)]
23. Mohamed, A.A.; Ricci, S.; Burini, A.; Galassi, R.; Santini, C.; Chiarella, G.M.; Melgarejo, D.Y.; Fackler, J.P., Jr. Halide and Nitrite Recognizing Hexanuclear Metallacycle Copper(II) Pyrazolates. *Inorg. Chem.* **2011**, *50*, 1014–1020. [[CrossRef](#)] [[PubMed](#)]
24. Li, H.-X.; Ren, Z.-G.; Liu, D.; Chen, Y.; Lang, J.-P.; Cheng, Z.-P.; Zhu, X.-L.; Abrahams, B.F. Single-crystal-to-single-crystal structural transformations of two sandwich-like Cu(II) pyrazolate complexes and their excellent catalytic performances in MMA polymerization. *Chem. Commun.* **2010**, *46*, 8430–8432. [[CrossRef](#)] [[PubMed](#)]
25. Yakovleva, M.A.; Kushan, E.V.; Boltacheva, N.S.; Filyakova, V.I.; Nefedov, S.E. Deprotonation of pyrazole and its analogs by aqueous copper acetate in the presence of triethylamine. *Russ. J. Inorg. Chem.* **2012**, *57*, 181–192. [[CrossRef](#)]
26. Di Nicola, C.; Garau, F.; Gazzano, M.; Guedes da Silva, M.F.C.; Lanza, A.; Monari, M.; Nestola, F.; Pandolfo, L.; Pettinari, C.; Pombeiro, A.J.L. New Coordination Polymers and Porous Supramolecular Metal Organic Network Based on the Trinuclear Triangular Secondary Building Unit $[\text{Cu}_3(\mu_3\text{-OH})(\mu\text{-pz})_3]^{2+}$ and 4,4'-Bypiridine. *Cryst. Growth Des.* **2012**, *12*, 2890–2901. [[CrossRef](#)]
27. Di Nicola, C.; Garau, F.; Gazzano, M.; Lanza, A.; Monari, M.; Nestola, F.; Pandolfo, L.; Pettinari, C.; Zorzi, F. Reactions of a Coordination Polymer Based on the Triangular Cluster $[\text{Cu}_3(\mu_3\text{-OH})(\mu\text{-pz})_3]^{2+}$ with Strong Acids. Crystal Structure and Supramolecular Assemblies of New Mono-, Tri-, and Hexanuclear Complexes and Coordination Polymers. *Cryst. Growth Des.* **2010**, *10*, 3120–3131. [[CrossRef](#)]
28. Zhou, Q.; Liu, Y.; Wang, R.; Fu, J.; Xu, J.; Lou, J. Synthesis, crystal structure and magnetic properties of a trinuclear Cu(II)-pyrazolate complex containing $\mu_3\text{-OH}$. *J. Coord. Chem.* **2009**, *62*, 311–318. [[CrossRef](#)]
29. Zhou, J.H.; Liu, Z.; Li, Y.Z.; Song, Y.; Chen, X.T.; You, X.Z. Synthesis, structures and magnetic properties of two copper(II) complexes with pyrazole and pivalate ligands. *J. Coord. Chem.* **2006**, *59*, 147–156. [[CrossRef](#)]
30. Davydenko, Y.M.; Demeshko, S.; Pavlenko, V.A.; Dechert, S.; Meyer, F.; Fritsky, I.O. Synthesis, Crystal Structure, Spectroscopic and Magnetically Study of Two Copper(II) Complexes with Pyrazole Ligand. *Z. Anorg. Allg. Chem.* **2013**, *639*, 1472–1476. [[CrossRef](#)]

31. Bala, S.; Bhattacharya, S.; Goswami, A.; Adhikary, A.; Konar, S.; Mondal, R. Designing Functional Metal–Organic Frameworks by Imparting a Hexanuclear Copper-Based Secondary Building Unit Specific Properties: Structural Correlations with Magnetic and Photocatalytic Activity. *Cryst. Growth Des.* **2014**, *14*, 6391–6398. [[CrossRef](#)]
32. Condello, F.; Garau, F.; Lanza, A.; Monari, M.; Nestola, F.; Pandolfo, L.; Pettinari, C. Synthesis and Structural Characterizations of New Coordination Polymers Generated by the Interaction Between the Trinuclear Triangular SBU $[\text{Cu}_3(\mu_3\text{-OH})(\mu\text{-pz})_3]^{2+}$ and 4,4'-Bipyridine. *Cryst. Growth Des.* **2015**, *15*, 4854–4862. [[CrossRef](#)]
33. Morgan, G.T.; Ackerman, I. CLII.—Substitution in the pyrazole series. Halogen derivatives of 3:5-dimethylpyrazole. *J. Chem. Soc. Trans.* **1923**, 123, 1308–1318. [[CrossRef](#)]
34. Hüttel, R.; Schäfer, O.; Jochum, P. Die Jodierung der Pyrazole. *Justus Liebigs Ann. Chem.* **1955**, 593, 200–207. [[CrossRef](#)]
35. Buchner, E.; Fritsch, M. VI. Darstellung und Derivate des freien Pyrazols. *Justus Liebigs Ann. Chem.* **1893**, 273, 256–266. [[CrossRef](#)]
36. Kahn, O. *Molecular Magnetism*; VCH Publishers: New York, NY, USA, 1993.
37. *Crystal Structure 4.2: Crystal Structure Analysis Package, Rigaku Corporation (2000–2015)*; Rigaku Corporation: Tokyo, Japan.
38. Dolomanov, O.V.; Bourhis, L.J.; Gildea, R.J.; Howard, J.A.K.; Puschmann, H. OLEX2: A complete structure solution, refinement and analysis program. *J. Appl. Cryst.* **2009**, *42*, 339–341. [[CrossRef](#)]
39. Sheldrick, G.M. Crystal structure refinement with SHELXL. *Acta Crystallogr. Sect. C Struct. Chem.* **2015**, *71*, 3–8. [[CrossRef](#)] [[PubMed](#)]
40. Macrae, C.F.; Edgington, P.R.; McCabe, P.; Pidcock, E.; Shields, G.P.; Taylor, R.; Towler, M.; Van De Streek, J. Mercury: Visualization and analysis of crystal Structures. *J. Appl. Crystallogr.* **2006**, *39*, 453–457. [[CrossRef](#)]
41. *POVRAY, Version 3.5*; Persistence of Vision Raytracer Pty. Ltd.: Williamstown, VIC, Australia, 2002.
42. Koch, W.; Holthausen, M.C. *A Chemist's Guide to Density Functional Theory*; VCH Publisher: Berlin, Germany, 2001.
43. Becke, A.D. Density-functional thermochemistry. III. The role of exact exchange. *J. Chem. Phys.* **1993**, *98*, 5648–5652. [[CrossRef](#)]
44. Frisch, M.J.; Pople, J.A.; Binkley, J.S. Self-consistent molecular orbital methods 25. Supplementary functions for Gaussian basis sets. *J. Chem. Phys.* **1984**, *80*, 3265–3269. [[CrossRef](#)]
45. Schmidt, M.W.; Baldridge, K.K.; Boatz, J.A.; Elbert, S.T.; Gordon, M.S.; Jensen, J.H.; Koseki, S.; Matsunaga, N.; Nguyen, K.A.; Su, S.; et al. General Atomic and Molecular Electronic Structure System. *J. Comput. Chem.* **1993**, *14*, 1347–1363. [[CrossRef](#)]
46. Addison, A.W.; Rao, T.N.; Reedijk, J.; van Rijn, J.; Verschoor, G.C. Synthesis, structure, and spectroscopic properties of copper(II) compounds containing nitrogen–sulphur donor ligands; the crystal and molecular structure of aqua[1,7-bis(N-methylbenzimidazol-2'-yl)-2,6-dithiaheptane]copper(II) perchlorate. *J. Chem. Soc. Dalton Trans.* **1984**, 7, 1349–1356. [[CrossRef](#)]
47. Yang, L.; Powell, D.R.; Houser, R.P. Structural variation in copper(I) complexes with pyridylmethylamide ligands: Structural analysis with a new four-coordinate geometry index, τ_4 . *Dalton Trans.* **2007**, 9, 955–964. [[CrossRef](#)] [[PubMed](#)]
48. Casarin, M.; Corvaja, C.; di Nicola, C.; Falcomer, D.; Franco, L.; Monari, M.; Pandolfo, L.; Pettinari, C.; Piccinelli, F.; Tagliatesta, P. Spontaneous Self-Assembly of an Unsymmetric Trinuclear Triangular Copper(II) Pyrazolate Complex, $[\text{Cu}_3(\mu_3\text{-OH})(\mu\text{-pz})_3(\text{MeCOO})_2(\text{Hpz})]$ (Hpz = Pyrazole). Synthesis, Experimental and Theoretical Characterization, Reactivity, and Catalytic Activity. *Inorg. Chem.* **2004**, *43*, 5865–5876. [[CrossRef](#)] [[PubMed](#)]
49. Heisenberg, W. Zur theorie des ferromagnetismus. *Z. Phys.* **1928**, *49*, 619–636. [[CrossRef](#)]
50. van Vleck, J.H.; Sherman, A. The Quantum Theory of Valence. *Rev. Mod. Phys.* **1935**, *7*, 167–228. [[CrossRef](#)]
51. Kambe, K. On the Paramagnetic Susceptibilities of Some Polynuclear Complex Salts. *J. Phys. Soc. Jpn.* **1950**, *5*, 48–51. [[CrossRef](#)]
52. Sinn, E. Magnetic Exchange in Polynuclear Metal Complexes. *Coord. Chem. Rev.* **1970**, *5*, 313–347. [[CrossRef](#)]
53. Bersuker, I.B. Modern aspects of the Jahn-Teller effect theory and applications to molecular problems. *Chem. Rev.* **2001**, *101*, 1067–1114. [[CrossRef](#)]
54. Cage, B.; Cotton, F.A.; Dalal, N.S.; Hillard, E.A.; Rakvin, B.; Ramsey, C.M. Observation of Symmetry Lowering and Electron Localization in the Doublet-States of a Spin-Frustrated Equilateral Triangular Lattice: $\text{Cu}_3(\text{O}_2\text{C}_{16}\text{H}_{23}) \cdot 1.2\text{C}_6\text{H}_{12}$. *J. Am. Chem. Soc.* **2003**, *125*, 5270–5271. [[CrossRef](#)]
55. Vreugdenhil, W.; Haasnoot, J.G.; Schoondergang, M.F.J. Reedijk, Spectroscopic and magnetic properties of transition metal(II) trifluoromethanesulfonate compounds with bridging asymmetric 3,4-dialkyl substituted 1,2,4-triazole ligands. *J. Inorg. Chim. Acta* **1987**, *130*, 235–242. [[CrossRef](#)]
56. Antolini, L.; Fabretti, A.C.; Gatteschi, D.; Giusti, A.; Sessoli, R. Synthesis, crystal and molecular structure, and magnetic properties of bis[tris(μ-3,5-diamino-1,2,4-triazole-N1,N2)tris(thiocyanato-N)nickel(II)]nickel(II) hexahydrate. *Inorg. Chem.* **1990**, *29*, 143–145. [[CrossRef](#)]
57. Antolini, L.; Fabretti, A.C.; Gatteschi, D.; Giusti, A.; Sessoli, R. Synthesis, crystal and molecular structure, and magnetic properties of bis[(μ-3,5-diamino-1,2,4-triazole-N1,N2-bis(μ-3,5-diamino-1,2,4-triazolato-N1,N2)triaquacobalt(II))]cobalt(III) trichloride nonahydrate. *Inorg. Chem.* **1991**, *30*, 4858–4860. [[CrossRef](#)]
58. Kolnaar, J.J.A.; van Dijk, G.; Kooijman, H.; Spek, A.L.; Ksenofontov, V.G.; Gütllich, P.; Haasnoot, J.G.; Reedijk, J. Synthesis, Structure, Magnetic Behavior, and Mössbauer Spectroscopy of Two New Iron(II) Spin-Transition Compounds with the Ligand 4-Isopropyl-1,2,4-triazole. X-ray Structure of $[\text{Fe}_3(4\text{-isopropyl-1,2,4-triazole})_6(\text{H}_2\text{O})_6](\text{tosylate})_6 \cdot 2\text{H}_2\text{O}$. *Inorg. Chem.* **1997**, *36*, 2433–2440. [[CrossRef](#)] [[PubMed](#)]

59. Garcia, Y.; van Koningsbruggen, P.J.; Lapouyade, R.; Fournès, L.; Rabardel, L.; Kahn, O.; Ksenofonov, V.; Levchenko, G.P.; Gütllich, P. Influences of Temperature, Pressure, and Lattice Solvents on the Spin Transition Regime of the Polymeric Compound $[\text{Fe}(\text{hyetrz})_3]_n \cdot 3\text{H}_2\text{O}$ (hyetrz = 4-(2'-hydroxyethyl)-1,2,4-triazole and $\text{A}^- = 3\text{-nitrophenylsulfonate}$). *Chem. Mater.* **1998**, *10*, 2426–2433. [[CrossRef](#)]
60. Roubeau, O.; Gomez, J.M.A.; Balskus, E.; Kolnaar, J.J.A.; Haasnoot, J.G.; Reedijk, J. Spin-transition behaviour in chains of Fe^{II} bridged by 4-substituted 1,2,4-triazoles carrying alkyl tails. *New J. Chem.* **2001**, *25*, 144–150. [[CrossRef](#)]
61. Spielberg, E.T.; Fittipaldi, M.; Geibig, D.; Gatteschi, D.; Plass, W. Electronic and magnetic structure of a triacetylphlorogucinol-bridged C_3 -symmetric trinuclear copper complex: Magnetic characterization, ESR spectroscopy, and DFT calculations. *Inorg. Chim. Acta* **2010**, *363*, 4269–4276. [[CrossRef](#)]
62. Shaik, S.; Hiberty, P.C. *A Chemist's Guide to Valence Bond Theory*; John Wiley & Sons: Hoboken, NJ, USA, 2007.
63. Garciabach, M.A.; Blaise, P.; Malrieu, J.P. Dimerization of polyacetylene treated as a spin-Peierls distortion of the Heisenberg Hamiltonian. *Phys. Rev. B Condens. Matter.* **1992**, *46*, 15645–15651. [[CrossRef](#)]
64. Mohamed, A.A.; Burini, A.; Galassi, R.; Paglialunga, D.; Galan-Mascaros, J.-R.; Dunbar, K.R.; Fackler, J.P., Jr. Self-assembly of a High-Nuclearity Chloride-Centered Copper(II) Cluster. Structure and Magnetic Properties of $[\text{Au}(\text{PPh}_3)_2][\text{trans-Cu}_6(\mu\text{-OH})_6\{\mu\text{-}(3,5\text{-CF}_3)_2\text{pz}\}_6\text{Cl}]$. *Inorg. Chem.* **2007**, *46*, 2348–2349. [[CrossRef](#)]
65. Borrás-Almenar, J.J.; Clemente-Juan, J.M.; Coronado, E.; Tsukerblat, B.S. MAGPACK A Package to Calculate the Energy Levels, Bulk Magnetic Properties, and Inelastic Neutron Scattering Spectra of High Nuclearity Spin Clusters. *J. Comput. Chem.* **2001**, *22*, 985–991. [[CrossRef](#)]
66. Rumer, G. Zum theorie der spinvalenz. *Nachr. Ges. Wiss. Göttingen Math. Phys. Kl.* **1932**, *1932*, 337–341.
67. Cimpoesu, F.; Chihaiia, V.; Stanica, N.; Hirao, K. The Spin Hamiltonian Effective Approach to the Vibronic Effects. Selected Cases. *Adv. Quant. Chem.* **2003**, *44*, 273–288. [[CrossRef](#)]
68. Pauling, L.; Wheland, G.W. The Nature of the Chemical Bond. V. The Quantum-Mechanical Calculation of the Resonance Energy of Benzene and Naphthalene and the Hydrocarbon Free Radicals. *J. Chem. Phys.* **1933**, *1*, 362–374. [[CrossRef](#)]
69. Ferbinteanu, M.; Buta, C.; Toader, A.M.; Cimpoesu, F. The spin coupling in the polyaromatic hydrocarbons and carbon-based materials. In *Carbon-Related Materials-in Recognition of Nobel Lectures by Prof. Akira Suzuki in ICCE*; Kaneko, S., Mele, P., Endo, T., Eds.; Springer: Cham, Switzerland, 2017; pp. 327–371. [[CrossRef](#)]
70. Toader, A.M.; Buta, C.M.; Frecus, B.; Mischie, A.; Cimpoesu, F. Valence Bond Account of Triangular Polyaromatic Hydrocarbons with Spin: Combining Ab Initio and Phenomenological Approaches. *J. Phys. Chem. C* **2019**, *123*, 6869–6880. [[CrossRef](#)]
71. Noodleman, L. Valence bond description of antiferromagnetic coupling in transition metal dimers. *J. Chem. Phys.* **1981**, *74*, 5737–5743. [[CrossRef](#)]
72. Noodleman, L.; Davidson, E.R. Ligand spin polarization and antiferromagnetic coupling in transition metal dimers. *Chem. Phys.* **1986**, *109*, 131–143. [[CrossRef](#)]
73. Ruiz, E.; Cano, J.; Alvarez, S.; Alemany, P. Broken symmetry approach to calculation of exchange coupling constants for homobinuclear and heterobinuclear transition metal complexes. *J. Comp. Chem.* **1999**, *20*, 1391–1400. [[CrossRef](#)]
74. Bencini, A.; Totti, F.; Daul, C.A.; Doclo, K.; Fantucci, P.; Barone, V. Density Functional Calculations of Magnetic Exchange Interactions in Polynuclear Transition Metal Complexes. *Inorg. Chem.* **1997**, *36*, 5022–5030. [[CrossRef](#)]
75. Shoji, M.; Koizumi, K.; Kitagawa, Y.; Kawakami, T.; Yamanaka, S.; Okumura, M.; Yamaguchi, K. A general algorithm for calculation of Heisenberg exchange integrals J in multispin systems. *Chem. Phys. Lett.* **2006**, *432*, 343–347. [[CrossRef](#)]
76. Ruiz, E. Theoretical study of the exchange coupling in large polynuclear transition metal complexes using DFT methods. In *Principles and Applications of Density Functional Theory in Inorganic Chemistry II. Structure and Bonding*; Springer: Berlin/Heidelberg, Germany, 2004; Volume 113, pp. 71–102. [[CrossRef](#)]
77. Atitoaie, A.; Tanasa, R.; Enachescu, C. Size dependent thermal hysteresis in spin-crossover nanoparticles reflected within a Monte Carlo based Ising-like model. *J. Magn. Magn. Mater.* **2012**, *324*, 1596–1600. [[CrossRef](#)]
78. Varret, F.; Salunke, S.A.; Boukheddaden, K.; Bousseksou, A.; Codjovi, É.; Enachescu, C.; Linares, J. The Ising-like model applied to switchable inorganic solids: Discussion of the static properties. *Comptes Rendus Chim.* **2003**, *6*, 385–393. [[CrossRef](#)]
79. Leininger, T.; Stoll, H.; Werner, H.-J.; Savin, A. Combining long-range configuration interaction with short-range density functionals. *Chem. Phys. Lett.* **1997**, *275*, 151–160. [[CrossRef](#)]
80. Kohn, W.; Meir, Y.; Makarov, D.E. van der Waals Energies in Density Functional Theory. *Phys. Rev. Lett.* **1998**, *80*, 4153. [[CrossRef](#)]
81. Iikura, H.; Tsuneda, T.; Yanai, T.; Hirao, K. A long-range correction scheme for generalized-gradient-approximation exchange functionals. *J. Chem. Phys.* **2001**, *115*, 3540–3544. [[CrossRef](#)]
82. Tsuneda, T.; Kamiya, M.; Hirao, K. Regional self-interaction correction of density functional theory. *J. Comput. Chem.* **2003**, *24*, 1592–1598. [[CrossRef](#)]
83. Grimme, S. Accurate description of van der Waals complexes by density functional theory including empirical corrections. *J. Comput. Chem.* **2004**, *25*, 1463–1473. [[CrossRef](#)] [[PubMed](#)]
84. Grimme, S.; Ehrlich, S.; Goerigk, L. Effect of the damping function in dispersion corrected density functional theory. *J. Comput. Chem.* **2011**, *32*, 1456–1465. [[CrossRef](#)]
85. Hay, P.J.; Thibault, J.C.; Hoffmann, R. Orbital interactions in metal dimer complexes. *J. Am. Chem. Soc.* **1975**, *97*, 4884–4899. [[CrossRef](#)]

-
86. Kahn, O.; Galy, J.; Journaux, Y.; Morgenstern-Badarau, I. Synthesis, crystal structure and molecular conformations, and magnetic properties of a copper-vanadyl (CuII-VOII) heterobinuclear complex: Interaction between orthogonal magnetic orbitals. *J. Am. Chem. Soc.* **1982**, *104*, 2165–2176. [[CrossRef](#)]
 87. Kahn, O. Magnetism of the Heteropolymetallic Systems. In *Theoretical Approaches; Structure and Bonding*; Springer: Berlin/Heidelberg, Germany, 1987; Volume 68. [[CrossRef](#)]
 88. Ruiz, E.; Alemany, P.; Alvarez, S.; Cano, J. Structural Modeling and Magneto– Structural Correlations for Hydroxo-Bridged Copper (II) Binuclear Complexes. *Inorg. Chem.* **1997**, *36*, 3683–3688. [[CrossRef](#)]